

ISOSTATIC COMPENSATION OF EQUATORIAL HIGHLANDS ON VENUS

Algis B. Kucinkas¹ and Donald L. Turcotte

Department of Geological Sciences, Cornell University, Ithaca, New York 14853

E-mail: algis@nomad.jpl.nasa.gov

Manuscript pages: 47

Figures: 8 numbered, 12 total

Tables: 2

Key words: Venus, isostasy, geoid, topography, Magellan

¹Currently at Jet Propulsion Laboratory, California Institute of Technology, Pasadena, Ca.

COMPENSATION OF EQUATORIAL HIGHLANDS ON VENUS

Send editorial correspondence and proofs to:

Algis B. Kucinskas

Jet Propulsion Laboratory/California Institute of Technology

Mail Stop 301-150

4800 Oak Grove Drive

Pasadena, CA 91109

ABSTRACT

We have used spherical harmonic models for Venus' global topography and gravity incorporating data from the Magellan mission to test isostatic compensation models in several equatorial highlands. A spectral study was conducted on the global harmonic models. We find that the power spectral density (PSD) of the Venus topography spectrum agrees quite well with a power - law scaling over a range in degree $1202 \ell \geq 3$ with a spectral slope $\beta \sim 2$ characteristic of Brown noise, similar to what is observed for the Earth's topography. However, for Venus the slope of the topography spectrum seems somewhat shallower than the Earth's and has significantly lower amplitudes which might reflect the dominant lowland topography on Venus. The low - degree part of the PSD for the Venus geoid anomaly also obeys a power-law with $\beta \sim -3$, consistent with Kaula's law for the Earth. For $\ell > 3$ the Venus geoid PSD shows larger amplitudes than for the Earth, a possible consequence of the strong correlations between gravity and topography on Venus. For Venus, degree geoid topography ratios (GTR) for a geoid resulting from uncompensated topography are significantly larger than degree GTRs for observed data, indicative of substantial compensation. Assuming a global Airy isostatic compensation mechanism at a single depth d , most of the observed topography is compensated at $d \sim 150$ km suggesting a thick lithosphere on Venus. Using the available harmonic models we then obtained $5^\circ \times 5^\circ$ mean values of Bouguer gravity for an uncompensated topography (Δg^u), and observed gravity anomalies (Δg), topography variations (h) and geoid anomalies (N) for five $30^\circ \times 30^\circ$ sample regions representative of the main classes of highlands found in the Venus equatorial zone. The samples included: the topographic swells of Beta and Atla Regiones, the high-plateaus of Ovda and Thetis Regiones, and a sample in the Chasmata area in central Aphrodite Terra. For each sample region, a line was fitted to the data values of Δg^u plotted against Δg with the slope defining a regional degree of compensation C . The N versus h data values for each sample were compared, in the least squares sense, to theoretical correlations for

Pratt, Airy, and thermal thinning isostasy models. **Isostatic** model parameters included: regional GTR and the corresponding depth of compensation W for the Pratt model, zero elevation **crustal** thickness (H) for the Airy model, and the thickness of the unperturbed (zero elevation) thermal lithosphere (y_{L_0}) for thermal compensation. We find that for **all** sample areas considered, C is high and the correlation of the h , N data presents strong coherence. For the Pratt and Airy model fits the respective parameter values are largest for the Beta and Atla swells. Parameter values are smallest for **Ovda** and Thetis with intermediate values for the **Chasmata** area. Although there are large variations in model parameters for the regional fits, the h , N data correlations in the chosen area.. can be explained by **isostatic** compensation models applicable on the Earth and involving variations in **crustal** (Airy) and/or **lithospheric** (thermal thinning) thicknesses. However, a thick zero - elevation thermal lithosphere (y_{L_0} - 300km) must be assumed for Venus. Compensation mechanisms **could** then be distributed among our chosen regions as follows: for **Ovda** and Thetis **Regiones** mainly Airy isostasy with H -50-60 km. For the **Chasmata** area sample Airy with perhaps a thermal component. Finally, a very strong thermal component for **Atla** and Beta. Aphrodite Terra, which shows a marked eastward increase in Pratt and Airy model parameters across its length, could be a candidate for thermal isostasy decay from east to west.

1. INTRODUCTION

Following the completion of the altimetry and cycle 4 gravity data acquisition phases of the **Magellan** mission to Venus high degree and order topography (120x 120) and **geopotential** (60 x 60) spherical harmonic models were produced (**Konopliv** et al, 1993). These models allow regional studies with spatial resolutions as small as -300 km. **Magellan** and Pioneer Venus Orbiter (**PVO**) tracking data used to produce the cycle 4 gravity model have poor resolution at high latitudes with respect to the spacecraft **periapsis**, a consequence of the large **ellipticity** of the spacecraft orbits. Because of this

an a priori constraint (Kaula's law) had to be applied for the estimation of the gravity model's harmonic coefficients thus making any quantitative interpretation of the high degree and order (ie small wavelength) part of this global gravity solution and of the derived high latitude regional gravity data unreliable. However, during the 70 day aerobraking experiment (which ended on August 6, 1993), the orbit of the **Magellan** spacecraft was quasi circularized using aerodynamic drag. Using preliminary cycle 5 (ie circular orbit) along with previous PVC) and cycle 4 Doppler tracking data a new 60 x 60 degree and order Venus **geopotential** spherical harmonic solution **was** recently produced (Konopliv and Sjogren, this issue). This latest model features lower overall uncertainties than previous cycle 4 models and higher resolution gravity data at high latitudes in certain areas of the planet (eg **Ishtar Terra**), with the highest resolution data still located in the equatorial zone.

Correlations between topography and gravity data sets gathered from orbiting spacecraft provide a basis for studying planetary interiors, especially when lacking in situ (e.g. seismological) data. Topography variations on a planet are the surface expression of a variety of geological and geophysical process and are generally compensated at long wavelengths. In the case of the Earth, topography highs are often isostatically compensated by low density roots. Anomalies in a planet's gravity or geoid (equipotential surface) are the consequence of variations in the distribution of mass at the planetary surface and in its interior. Whereas local (i.e. small wavelength) gravity anomalies better describe local uncompensated topography variations, anomalies in the geoid are best suited to study the compensation associated with longer wavelength regional topography anomalies. Indeed, if regional topography is compensated **then** it directly correlates with **the** geoid anomalies for the considered region (Turcotte and Schubert, '1982). Thus to learn more about the compensation mechanisms and internal evolution for a terrestrial planet it is useful to correlate geoid and topography data sets at long wavelengths.

Explaining the support (ie compensation) mechanism of the high topography on Venus is of critical importance for testing the predictions of models describing the thermal structure and evolution of the planet. It is now common practice to consider two classes of mechanisms for explaining the high topography on Venus. First, one can consider isostatic compensation models. Assuming Airy isostasy, many highlands on Venus have large apparent depths of compensation (ADC) thus requiring a thick lithosphere. This led several authors (Phillips, 1990; Kieffer and Hager, 1991; Bindshadler et al, 1992 a,b) to consider a second class of models associated with the dynamic support of topography through the pressure gradients associated with mantle convection. These models imply a hot, thin lithosphere with steady-state heat loss. However, it can be argued whether convection on Venus can indeed support the topography and associated gravity (or geoid) anomalies. Large amplitude dynamic topography on Venus requires high pressures (convective stresses) associated with high mantle viscosities and low mantle temperatures. But, using parametrized convection (Turcotte 1980), arguments can be made for a lower mantle viscosity on Venus than on the Earth leading to higher values of the Rayleigh number (Turcotte, 1993). Also, on the Earth there is little evidence for significant dynamic topography. Indeed, essentially all terrestrial high topography can be explained isostatically in terms of variations in crustal or lithospheric thicknesses. On Earth, high topography is associated with a thick, strong lithosphere.

In this work we use the 120 X 120 Venus topography model and the newly released 60 x 60 Venus geopotential model incorporating the most recent cycle 5 tracking data to obtain a series of averaged point values of topography (h) and geoid (N) anomalies for several regions characteristic of the equatorial highlands of Venus (namely in Beta Regio and Aphrodite Terra). We then examine the N and h data for each sample region in terms of theoretical h, N correlations for Pratt, Airy, and thermal isostatic compensation models. In section 11 we discuss harmonic models for Venus' topography

and **geopotential**. In section 111 we analyze the power spectrum derived from the topography and **geoid** spectra in terms of power - law scaling and compare these results to that obtained for the Earth's spectra. We then compare degree **geoid** to topography ratios (**GTR**) to theoretical degree **GTR**'s for a global **isostatic** compensation model at a single depth and for uncompensated global topography. In section IV we introduce the three **isostatic** compensation models and relevant model parameters which we fit to the h, N anomaly data observed in each of the chosen sample **areas**. Finally, results of the three model fits to the regional data are **presented** and discussed in section V.

11. SPHERICAL HARMONIC MODELS FOR VENUS

In what follows we consider a frame of reference rotating with the planet and the origin of coordinates at the center of mass of the planet,

It is standard practice to expand data sets on a planetary surface in a uniformly convergent double series of surface spherical harmonics of degree ℓ and order m (Heiskanen and Moritz, 1967). For surface topography the radius R of the planet is given by:

$$R(\theta, \varphi) = R_t \left[1 + \sum_{\ell=1}^{\ell_{\max}} \sum_{m=0}^{\ell} (\bar{A}_{\ell m} \cos m \varphi + \bar{B}_{\ell m} \sin m \varphi) \bar{P}_{\ell m}(\sin \theta) \right] \quad (1)$$

where R_t is a reference radius, ℓ_{\max} is the maximum degree considered (characterizing the resolution of the expansion), θ and φ are the latitude and longitude, $\bar{A}_{\ell m}$ and $\bar{B}_{\ell m}$ are the fully normalized dimensionless Stokes harmonic coefficients characterizing the surface and $\bar{P}_{\ell m}$ are the associated Legendre functions fully normalized with:

$$1/4\pi \int_0^{2\pi} \int_{-1}^1 \bar{P}_{\ell m}^2(\sin \theta) \left. \begin{matrix} \cos^2 m\varphi \\ \sin^2 m\varphi \end{matrix} \right\} d(\sin \theta) d\varphi = 1 \quad (2)$$

$R - R_t$ then represents the variations in topography with respect to a reference sphere of radius R_t . Similarly, for the gravitational potential $U(r, \theta, \varphi)$ at a point outside the planet, we have:

$$u(r, \theta, \varphi) = \frac{GM}{r} \left[1 + \sum_{\ell=2}^{\ell_{\max}} \sum_{m=0}^{\ell} \left(\frac{R_g}{r} \right)^{\ell} (\bar{C}_{\ell m} \cos m \varphi + \bar{S}_{\ell m} \sin m \varphi) \bar{P}_{\ell m}(\sin \theta) \right] \quad (3)$$

where G is the universal gravitational constant, M the mass of the planet, R_g is a reference radius for the geopotential expansion, r is the radial distance of the considered external point with respect to the body - fixed coordinate system, $\bar{C}_{\ell m}$ and $\bar{S}_{\ell m}$ are the fully normalized dimensionless harmonic coefficients of the gravity field, and the $\bar{P}_{\ell m}$ are normalized as in Eq. (2). There are no terms in $\ell = 1$ in Eq. (3) as a consequence of the choice for the origin of coordinates.

If $R_t > R_g$, it is convenient to rescale the gravity harmonic coefficients to the reference radius R_t , This can be done by multiplying the $\bar{C}_{\ell m}$ and $\bar{S}_{\ell m}$ by the resealing factor $(R_g / R_t)^{\ell}$, for all ℓ and m . From here on we assume the $\bar{C}_{\ell m}$ and $\bar{S}_{\ell m}$ are rescaled values, with $R_o = R_t = R_g$ in the expansions we consider.

If one introduces U^* the gravitational potential of a reference ellipsoid expressed as a spherical harmonic expansion with $\bar{C}_{2\ell 0}^*$ terms only (Balmino, 1986) we can then define an anomalous (or disturbing) potential T as :

$$T = U - U^* = \frac{GM}{r} \left[\sum_{\ell=2}^{\ell_{\max}} \sum_{m=0}^{\ell} \left(\frac{R_o}{r} \right)^{\ell} (\Delta \bar{C}_{\ell m} \cos m \varphi + \Delta \bar{S}_{\ell m} \sin m \varphi) \bar{P}_{\ell m}(\sin \theta) \right] \quad (4)$$

where $\Delta \bar{C}_{\ell m} = \bar{C}_{\ell m} - \bar{C}_{\ell m}^*$ if $m = 0$ and ℓ even, $\Delta \bar{C}_{\ell m} = 0$ otherwise and $\Delta \bar{S}_{\ell m} = \bar{S}_{\ell m}$. The geoid anomaly (or height) N with respect to the reference geoid can then be obtained via Bruns' formula as (Heiskanen and Moritz, 1967): $N = T/\gamma$, $\gamma(\theta)$ being the "normal"

gravity of the reference ellipsoid at a point (r, θ, φ) On the reference ellipsoid. Now, in the spherical approximation, we can formally (but not geodetically) treat the reference ellipsoid as a sphere of radius R_0 in equations relating quantities of the anomalous field (ie the flattening is neglected); in the case of the geoidal anomalies for the Earth, the error in doing so is only $\sim 3 \times 10^{-3} N$, ie less than 1 m for $N=100\text{m}$ (Heiskanen and Moritz, 1967; Moritz, 1980) which is quite acceptable for the purpose of our study. In this approximation, we thus have:

$$N(\theta, \varphi) = R_0 \left[\sum_{\ell=2}^{\ell_{\max}} \sum_{m=0}^{\ell} (\Delta \bar{C}_{\ell m} \cos m \varphi + \Delta \bar{S}_{\ell m} \sin m \varphi) \bar{P}_{\ell m}(\sin \theta) \right] \quad (5)$$

The gravity anomaly Δg can be obtained from the disturbing potential T as (Heiskanen and Moritz, 1967):

$$\Delta g = - \frac{\partial T}{\partial r} - \frac{2T}{r} \quad (6)$$

which yields, after substituting T from Eq. (4) in Eq. (6)

$$\Delta g = \frac{GM}{r^2} \left[\sum_{\ell=2}^{\ell_{\max}} \sum_{m=0}^{\ell} \left(\frac{R_0}{r} \right)^{\ell} (\ell-1) (\Delta \bar{C}_{\ell m} \cos m \varphi + \Delta \bar{S}_{\ell m} \sin m \varphi) \bar{P}_{\ell m}(\sin \theta) \right] \quad (7)$$

In the spherical approximation, Eq. (7) then becomes

$$\Delta g = \frac{GM}{R_0^2} \left[\sum_{\ell=2}^{\ell_{\max}} \sum_{m=0}^{\ell} (\ell-1) (\Delta \bar{C}_{\ell m} \cos m \varphi + \Delta \bar{S}_{\ell m} \sin m \varphi) \bar{P}_{\ell m}(\sin \theta) \right] \quad (8)$$

Long wavelength (ie small ℓ) geoidal undulations (anomalies) N are amplified relative to gravity anomalies Δg ; indeed, it can be shown (Watts and Daly, 1981; Lliboutry, 1982) that, in the spherical approximation:

$$\Delta g_{\ell m} / g_o = (\ell - 1) N_{\ell m} / R_o \quad (9)$$

with:

$$g_o = \frac{GM}{R_o^2}, \quad \Delta g_{\ell m} = \frac{GM}{R_o^2} (\ell - 1) \begin{Bmatrix} \Delta \bar{C}_{\ell m} \\ \Delta \bar{S}_{\ell m} \end{Bmatrix}, \quad \text{and} \quad N_{\ell m} = R_o \begin{Bmatrix} \Delta \bar{C}_{\ell m} \\ \Delta \bar{S}_{\ell m} \end{Bmatrix} \quad (10)$$

For large values of ℓ (ie small wavelengths) geoidal undulations smooth out gravity anomalies as $1/(\ell-1)$. Thus for studying density anomalies at depth it is more useful to study geoid anomalies on a regional scale (ie wavelengths greater than a few hundred km).

In this paper we use a new 120x120 spherical harmonic model for Venus' topography produced at the Jet Propulsion Laboratory (JPL) (Konopliv et al, 1993; Rappaport, 1994). The normalized spherical harmonic coefficients of the topography model were individually computed by numerical quadrature over the surface of Venus from a grid of averaged planetary radii (grid spacing of 10, obtained from the complete set of Pioneer Venus Orbiter (PVO) and Magellan altimetry data (Ford and Pettengill, 1992). The mean reference radius obtained for this model is $R_t = 6051.839$ km. The model is illustrated in Fig. 1a which shows a contour map of the observed variations for Venus topography above and below the reference radius R_t . For consistency with the geoid anomaly map of Fig. 1b the topography expansion was truncated at degree and order 60.

We also make use of a 60 x 60 spherical harmonic model for the Venus geopotential (namely "MGNP60FSAAP") recently obtained by Konopliv and Sjogren (this issue). The fully normalized harmonic coefficients for this model were estimated using JPL's Double Precision Orbit Determination Program (DPODP) (Moyer, 1971), from the combined two-way coherent Doppler shift data from the tracking observations

of the PVO spacecraft (S-band data) and the **Magellan** spacecraft (higher resolution X-band data). The **Magellan** data include global cycle 4 tracking data and cycle 5 quasi circular orbit (197 km periapsis altitude, apoapsis 540 km) high resolution tracking data in a longitude band extending from -90° W to $+20^\circ$ E. For this model the reference radius is $R_g = 6051.0$ km. We first resealed the **geopotential** coefficients to the reference radius of the topography model (ie to $R. = R_t$) and then derived the harmonic coefficients for the **geoid** anomaly N in the spherical approximation using Eq. (5). For Venus, the reference ellipsoid is taken to be (in the geometrical sense here) a sphere of radius R_o , so that $\Delta\bar{C}_{lm} \equiv \bar{C}_{lm}$ (ie flattening $f=0$). A contour map of the variations in the height of the Venus **geoid** with respect to the reference **geoid** is given in Fig. 1b. The strong positive correlation between Venus topography and **geoid** (Phillips et al., 1979; Sjogren et al. 1980) is readily apparent in Fig. 1a and 1b.

Both the PVO spacecraft and **Magellan** spacecraft (in cycle 4) moved in very excentric orbits while raw Doppler tracking data was being acquired. As a consequence, the highest resolution (~ 200 km) gravity data was obtained at latitudes close ($\sim \pm 30^\circ$) to spacecraft periapsis (15° N for PVO, 10° N for **Magellan**) and the lowest resolution gravity data near the poles (eg Ishtar Terra was poorly resolved). Although the cycle 5 data in the **MGNP60FSAAP** solution is still incomplete, this new model provides improved harmonic coefficient estimates and higher resolution in the polar regions corresponding to the longitude band of the current cycle 5 data coverage. This is especially true in the Northern latitudes with Ishtar Terra's resolution now greatly improved. Because **MGNP60FSAAP** also incorporates PVO and cycle 4 data, which include a large difference in resolution with latitude, the application of an a priori constraint in the estimation of the high degree and order harmonic coefficients is still required. Without this constraint the solution is unstable above degree and order ~ 25 . However, when generating the harmonic coefficients of the **PMGN60FSAAP** solution, the bias was applied locally; namely, surface accelerations resulting from a biased

(Kaula's law) harmonic model were used as input to the ODP program only for regions where uncertainties in the gravity data were highest (Konopliv and Sjogren, this issue). Both a biased (ie with Kaula a priori locally applied) and a non biased solution were generated. For the latter solution, the formal error in the geoidal undulations (anomalies) is still smallest in an equatorial band extending $\sim\pm 30^\circ$ about periapsis of the Magellan spacecraft (Konopliv and Sjogren, this issue).

In the following section we will restrict our global analysis of the geoid spectrum to the lower degree part, and in section V, for our regional study of topography and geoid data correlations, we will focus on the area where the highest resolution raw gravity data was acquired, namely the equatorial latitudes.

111. GLOBAL SPECTRAL STUDY

The discrete (degree) power spectrum of a given field (geophysical quantity) observed on a planetary surface and expanded in a spectrum of surface spherical harmonics summarizes information on the wavelength characteristics (variations) of the field (Lambeck, 1988). We define the degree variance of the harmonic spectra of the topography and geoid as:

$$V_\ell^t = R_o^2 \sum_{m=0}^{\ell} (\bar{A}_{\ell m}^2 + \bar{B}_{\ell m}^2) \quad (11)$$

for the topography, and:

$$V_\ell^n = R_o^2 \sum_{m=0}^{\ell} (\Delta C_{\ell m}^2 + \Delta S_{\ell m}^2) \quad (12)$$

for the geoid anomaly, where $R_o = R_t$ for the Venus data. We then define the degree Power Spectral Density (PSD) for these expansions as: $P_\ell^t = V_\ell^t/k_o = \lambda_o V_\ell^t$ for the topography, and $P_\ell^n = V_\ell^n/k_o = \lambda_o V_\ell^n$ for the geoid variations, where $\lambda_o = 2\pi R_o$ is the

wavelength over which data are included in the expansions and $k_\ell = 1/\lambda_\ell = \ell/2\pi R_o$ is the wave number.

For the topographic variance spectrum of the Earth it has been noted (Vening - Meinesz, 1951) that $V_\ell^t \sim \ell^{-2}$. Similarly, for the Earth's geopotential there is also a systematic dependence on degree for the variance spectrum $V_\ell^g \sim \ell^{-3}$, known as Kaula's law. In our notation, for the Earth's geoid PSD, Kaula's law is: $P_\ell^n \sim \ell^{-3}$ or, alternatively, $P_\ell^n \sim k_\ell^{-3}$. Such a dependence on ℓ for the Earth's gravity spectrum has been attributed to a random distribution of density anomalies at depth (Lambeck, 1976; Kaula, 1977). A spherical harmonic representation is said to be statistically scale invariant over a given range in wavelength if its PSD has a power-law dependence on wave-number (Turcotte, 1987; Kucinskis et al., 1992): $P_\ell(k_\ell) = Ck_\ell^{-\beta}$, $\beta > 0$ and C being constants ($-\beta$ is the slope).

In Fig.2a and 2b we give the degree PSD (in km³) for the global topography of Venus ($\ell_{\max} = 120$) and the Earth ($\ell_{\max} = 180$) plotted against k_ℓ (in km⁻¹) in a log - log scale (open circles). The PSD spectrum for Venus was obtained using the 120 x 120 model of Rappaport (1994) and that for the Earth using the "ETOPO 5" 180 x 180 model of Rapp (1982; 1989). The Earth's harmonic model is for "equivalent rock topography" (Balmino et al, 1973; Pavlis and Rapp, 1990) with a reference radius $R = 6371.0$ km. The fully normalized model coefficients were computed from 1° x 10 mean elevations and depths.

For $\ell < 3$ the Venus topography spectrum shows a rollover. This is also observed for the Earth topography but the power deficiency starts at a higher degree $\ell = 5$. We then model the decay of the PSD spectra for each of the two planetary topographies as $Ck_\ell^{-\beta}$ by performing a linear least squares fit of the log-log spectra over a degree range $120 \geq \ell \geq 3$ for Venus and $180 \geq \ell \geq 5$ for the Earth. Results of the fits, namely the slope $-\beta$ and intercept $K = \log_{10} C$, are given in Table I.

Over the respective degree intervals for the fits, we see that both the Venus and Earth topography data agree well with a power-law spectral correlation with $\beta = 2$ (solid correlation lines in Fig. 2a and 2b). This correlation is characteristic of Brown noise, with amplitudes directly proportional to wavelengths and the height to width (ie aspect) ratios of elevated features of various scales being the same. We also note that the Venus spectrum has **significantly** lower amplitude values than that for the Earth data and that the Venus topography **spectral slope** is slightly shallower than the Earth's ($\beta \sim 1.7$ versus $\beta \sim 2$). This confirms with the **Magellan** data a result reported earlier by other authors who compared the Earth's topography with **PVO** Venus altimetry (Kaula, 1984; Turcotte, 1987). For Venus, the **hypso**metric histogram is **unimodal** whereas the Earth's is **bimodal** (McGill et al, 1983). Indeed, there is a predominance of "rolling plains" topography on Venus with more than 80% of the surface lying within 1 km of the mean planetary radius (6051.839 km) (Masursky et al, 1980; Phillips et al, 1981; Ford and Pettengill, 1992). Kaula (1984) sees in this confinement of regions of marked topography anomalies to a few regions on the planet an explanation for the smaller amplitudes and shallower spectral slope observed for the Venus topography spectrum.

We show the degree PSD (in m^3) for the Venus and Earth geoid anomaly data in Fig. 3a and 3b, plotted versus k_l (in km^{-1}) on a log-log scale. The spectra were obtained using the 60x60 harmonic geopotential model of Konopliv and Sjogren (this issue) for Venus and for the Earth using the JGM-2, 70x70 geopotential model from the Topex/Poseidon mission (Nerem et al., 1994). The geoid anomaly for the Earth model was determined using Eq. (5) and with respect to a reference ellipsoid with an equatorial radius of 6378.1363 km and a flattening $f = 1/298.2570$ as a best fit to the Earth's geoid. In Fig. 3b the PSD values for the Earth geoid anomaly are plotted as open circles symbols.' For the Venus geoid undulations in Fig. 3a, we plotted PSD values corresponding to the biased (ie with Kaula a-priori) 60x60 geopotential solution "MGNP60FSAAP" as open circle symbols and PSD values corresponding to the unbiased

(ie with no **Kaula** a-priori) solution as dots. We notice that the unbiased spectrum still diverges from $\ell - 25$ as the no-bias **geopotential** solution becomes unstable. Also, it is seen that for the **biased** model's PSD there is a noticeable drop in the spectrum at degree $\ell - 25$ a consequence of the a-priori constraint when estimating high degree and order coefficients. We further note that the **geoid** spectrum for Venus presents a rollover at the same degree $\ell - 3$ as its topography counterpart. The Earth's **geoid** spectrum also presents a change in slope at low degrees, but the cutoff is less clear.

We also performed a linear least squares fit corresponding to the $Ck_{\ell}^{-\beta}$ model to the log-log **geoid** spectra of Venus and the Earth over the ranges of $252 \leq \ell \leq 3$ and $702 \sim 23$ respectively. From the results of the fits in Table I we see that Venus and Terrestrial **geoid** data indicate the application of a power-law scaling (solid correlation lines in Fig. 3a and 3b) over the range in degree of each fit. For both the Venus and Earth **geoids** we obtain $\beta - 3$, consistent (within experimental scatter) with Kaula's law. Also, for $\ell > 3$ the Venus **geoid** PSD has larger amplitudes than Earth data, a possible consequence of the strong positive correlation between gravity and topography on Venus (Phillips and Malin, 1983).

For given **geopotential** and topography harmonic expansions we define a corresponding degree **geoid to topography ratio** (GTR) as: $GTR_{\ell} = (V_{\ell}^g / V_{\ell}^t)^{1/2}$, estimated in this paper in units of m/km. GTR's from observed data can then be compared to theoretical GTR's derived for various simple compensation models so as to test the validity of the models and place constraints on the global average compensation mechanisms for the planet.

For a classic two layer model with planetary surface topography **isostatically** compensated at a single global depth of compensation d the spherical harmonic coefficients for the resulting "topographic **isostatic**" model **geopotential** are given, in a spherical geometry and to first order, by (Rummel et al, 1988; Rapp, 1989):

$$\begin{pmatrix} C_{\ell m}^i \\ S_{\ell m}^i \end{pmatrix} = \frac{3}{2\ell+1} \frac{\rho_c}{\bar{\rho}} \left[1 - \left(\frac{R_o - d}{R_o} \right)^\ell \right] \begin{pmatrix} \bar{A}_{\ell m} \\ \bar{B}_{\ell m} \end{pmatrix} \quad (13)$$

where R_o is the mean planetary radius, ρ_c is the surface (crustal) density and $\bar{\rho}$ the mean planetary density with $\bar{\rho} = 3M/4\pi R_o^3$. For Venus, we take $\rho_c = 2.9 \text{ g/cm}^3$, and $\bar{\rho} = 5.244 \text{ g/cm}^3$ (McNamee et al., 1993). This theoretical geopotential corresponds to an Airy isostatic model at a global compensation depth d or, equivalently, to a Pratt isostatic compensation at depth $W = 2d$ (Dahlen, 1982; Hager, 1983; Bills et al., 1987).

For uncompensated topography, the harmonic coefficients of the resulting (Bouguer) geopotential are given by:

$$\begin{pmatrix} C_{\ell m}^u \\ S_{\ell m}^u \end{pmatrix} = \frac{3}{2\ell+1} \frac{\rho_c}{\bar{\rho}} \begin{pmatrix} \bar{A}_{\ell m} \\ \bar{B}_{\ell m} \end{pmatrix} \quad (14)$$

Using the spherical harmonic coefficients for the isostatic geopotential model in Eq. (11) we can introduce the degree variance $V_\ell^{n,i}$ for the geoid anomaly of an isostatic compensation model at depth d . Then, the corresponding isostatic compensation degree GTR is just: $GTR_\ell^i = (V_\ell^{n,i}/V_\ell^t)^{1/2}$ where V_ℓ^t is the degree variance for the observed global topography. Similarly, for uncompensated topography, the degree GTR is: $GTR_\ell^u = (V_\ell^{n,u}/V_\ell^t)$, with $V_\ell^{n,u}$ the degree variance for an uncompensated topography model geoid anomaly. In what follows GTR_ℓ will denote the degree GTR for the observed geoid and topography data,

In Fig. 4 we plot the degree GTR (in m/km) for Venus versus degree ℓ (with $\ell_{\max} = 60$) in a log-linear scale for both the observed data (open circles) and an uncompensated topography model (solid curve). It is seen that the GTR_ℓ^u ratios are much larger than the observed GTR_ℓ values for all ℓ . At long wavelengths ($\lambda \sim 1,400 \text{ km}$) we find the observed geoid signal to be - 15% of the uncompensated topography geoid

signal. Thus, much of the observed geoid anomalies can be directly associated with compensated topography.

In Fig. 5 we show the degree GTR_l^j plotted versus l (with $l_{\max} = 60$) for Airy isostasy models with compensation at depths of 50, 150 and 300 km (solid curves). The observed degree GTR_l are also plotted (open circles). We believe the drop in GTR_l occurring from $l \sim 20$ is an artifact due to the a-priori constraint used to estimate the coefficients of the Venus geopotential. This phenomenon was noted earlier in the decay of the Venus geoid PSD. Given this we think there is reasonable agreement, for most values of $l > 6$, between the observed data points and an Airy model curve with a global depth of compensation $d = 150$ km. To test this further we plotted in Fig. 3a (as a dashed curve) the degree PSI for an Airy model geoid corresponding to Venus topography compensated at a depth of 150 km. Except for the lowest degrees there is good agreement with the $\beta - 3$ correlation line we fitted to the low degree part of the observed geoid data. Thus, for the Venus data, assuming a global Airy isostatic compensation mechanism at a single depth, most of the observed topography is compensated at depths in excess of 100 km thus implying a thick crust and lithosphere on Venus. In the case of the Earth, a good agreement with the observed geopotential PSD is found for an Airy-model PSD with $d=50$ km (Rapp, 1982; Rummel et al, 1988).

IV. ISOSTATIC COMPENSATION MODELS

Density variations within the lithosphere of a planet contribute significantly to the observed surface gravity and geoid anomalies. Over shorter wavelengths topography (with crustal density ρ_c) is essentially uncompensated and correlates with the corresponding local gravity anomaly Δg^u through the Bouguer gravity formula (Turcotte and Schubert, 1982, equation 5-11 1). Over larger wavelengths (a few hundred km for the Earth), topography can be expected to be largely compensated. In the case of the Earth, high topography is generally associated with a thick, strong lithosphere. Essentially all

terrestrial topography can be explained either by changes in **crustal** thickness associated with **Airy isostasy** (as for the continents or some oceanic plateaus) or by variations in **lithospheric** thickness associated with **thermal isostasy** as is the case for mid-ocean ridge **bathymetry** (thickening of a cooling, ocean lithosphere by conductive heat transport to the surface) and for continental and oceanic **intraplate** hot-spot swells (**lithospheric thinning**) (Turcotte, 1989),

In regions of isostatic or hydrostatic equilibrium (HE) the net mass in vertical columns of material must be equal. In terms of the density distribution $\Delta\rho$ in the lithosphere this condition can be written as (Haxby and Turcotte, 1978):

$$\int_0^{t_c} \Delta\rho(y) dy = 0 \quad (15)$$

where t_c is the thickness of the considered column of material and y is the vertical coordinate (or depth). Thus, while the study of gravity anomalies is indeed important for determining the relationship between gravity and local topography (**Bouguer** formula) and to tell us to what extent a given region is **isostatically** compensated, gravity anomalies are not the best sources of information on the dependency of density on depth and on the mechanisms of compensation operating in the lithosphere. This is accomplished much better by the study of the perturbations in a planet's **equipotential** surface (**geoid**).

Indeed, using the technique of matched asymptotic expansions, Ockendon and Turcotte (1977) showed that **geoidal** anomalies or undulations are non zero in **isostatically** compensated regions and measure the dipole moment of the local density distribution below the **point** of observation. In the case of a shallow, long wavelength isostatic **density** distribution $\Delta\rho$ the resulting **isostatic** geoid anomaly N is directly proportional to the dipole moment of the local density distribution according to (Haxby and Turcotte, 1978):

$$N = - \frac{2\pi G}{g_0} \int_0^{t_c} y \Delta\rho(y) dy \quad (16)$$

where g_0 is the “normal gravity” or the gravity acceleration for the reference ellipsoid measured on the reference **geoid**, G is the universal constant of gravitation, and t_c and y are as defined in Eq. (15). For the **Earth** this relationship (often referred to in the literature as the “HOT” equation) is usually a good approximation for wavelengths larger than a few hundred km, when there is near total **isostatic** compensation.

Once a density model distribution is assumed and a reference state is defined the HE and HOT relationships yield a theoretical expression for N in terms of observed h which can then be compared, in a forward modeling approach, to observed regional values of N to get a better understanding of the (a priori unknown) local state of compensation and estimate compensation model parameters. In this investigation, mean values of observed N and h data for each of our sample equatorial regions on Venus were compared to theoretical h , N correlations for three isostatic compensation models: Pratt, Airy, and thermal thinning of the Venusian lithosphere. The three models and their main parameters are illustrated in the diagrams of Fig. 6.

(a) Pratt-Hayford Compensation Model

For the Pratt-Hayford model isostatic compensation and thus support of high surface topography is achieved by a mass column with horizontal variations in density over a prescribed “depth of compensation” W (that is a constant **crustal** thickness). This model is illustrated by the diagram in Fig. 6a. Here, the variable density ρ_i of a given column i is related to the elevation h above the reference level by the isostatic relationship (HE) of Eq. (15) as:

$$\rho_i = \rho_0 W / (W + h) \quad (17)$$

where p_0 is the density of the reference column (ie with *zero* elevation with respect to the reference surface). Then, using Eq. (16) (ie the HOT relationship) and HE to eliminate ρ_i , and taking crust with zero elevation as the reference level or “state” the local Pratt geoid anomaly N_{Pratt} associated with the compensated observed topography variation h is given by:

$$N_{Pratt} = \frac{\pi G}{g_0} p_0 W h \quad (18)$$

with g_0 and G defined above. The Pratt geoid anomaly is a linear function of the topography variation. One can then define the local geoid to topography ratio. (GTR) as:

$$GTR = N_{Pratt} / h \quad (19)$$

and thus express the depth of compensation W as a linear function of GTR using Eq. (18) as:

$$W = GTR (g_0 / \pi G \rho_0) \quad (20)$$

On the Earth W approximately corresponds to the depth to the asthenosphere (ie the thermal lithosphere thickness). In this paper ρ_0 is the density ρ_m of the Venus mantle, with $p_0 = \rho_m = 3300 \text{ kg m}^{-3}$ (Turcotte, 1993), and $g_0 = GM/R_0^2 = 8.87 \text{ m S}^{-2}$. GTR is given in m/km and W in km.

(b) Airy - Heiskanen Compensation Model

Next we considered an Airy - Heiskanen compensation mechanism, shown in the Fig. 6b diagram. Here the surface topography is isostatically compensated by low and constant density crustal roots which replace higher density mantle rock. The thickness of

the must with zero elevation with respect to the reference level (sphere of radius R_0 here) is noted as H . From the principle of hydrostatic equilibrium (HE) in Eq. (15) the thickness of the root b is related to the **crustal** elevation h as:

$$b(h) = \rho_c h / (\rho_m - \rho_c) \quad (21)$$

with ρ_c the **crustal** density and ρ_m the underlying mantle density. Then, taking for the reference state the continental crust with zero elevation and using Eq. (17) to substitute for b , the Airy geoid anomaly associated with the compensated topography h is obtained from Eq. (16) (HOT formula) as:

$$N_{\text{Airy}} = \frac{\pi G \rho_c}{2} \left[2 H h + \frac{\rho_m}{(\rho_m - \rho_c)} h^2 \right] \quad (22)$$

For the Airy correlation, N is a quadratic function of elevation h . We took $\rho_c = 2900 \text{ kg m}^{-3}$ for the Venus **crustal** density based on Venusian surface rock densities as measured by the Venera Landers (Surkov et al, 1984).

(c) *Thermal Compensation Model*

Finally, we considered thermal isostasy with lithospheric thinning. For this model, illustrated in Fig. 6c, we are concerned with compensation/support of topography associated with thermal thinning (by conductive heat transport) of the lower lithosphere. Here, part of the thermal lithosphere has been converted into hot, low density **asthenosphere** due to heating from below (eg basal heating from ascending mantle plumes). This results in an elevation (thermal swell or uplift) of the lithosphere's upper surface due to thermal expansion, while at the same time the density of the lower lithospheric material decreases as it is replaced by hot **asthenospheric** material. This low density material supports the surface swell in a way analogous to Airy compensation's

crustal roots (Crough, 1978; Morgan and Phillips, 1983; Smrekar and Phillips, 1991). In what follows we will assume as a first order approximation that there is no heat production (sources) in the Venusian lithosphere. This is valid if the concentration of heat producing elements in the crust is less than 20% of the total and the lithosphere thickness is small compared to that of the Venus mantle (Turcotte, 1993). We also assume here that the lithosphere is a conductive layer atop an **asthenosphere** (upper part of the mantle) which is convecting and isothermal (temperature T_m). The surface temperature T_s and the thermal parameters of the Venus lithosphere are considered constant in time.

In this work we assume the temperature distribution (profile) T in the Venusian lithosphere has an error function dependence on depth which can be written as (Turcotte and Schubert, 1982):

$$\frac{T_m - T}{T_m - T_s} = \text{erfc} \left[\frac{y}{2 (\kappa t)^{1/2}} \right] \quad (23)$$

where erfc is the **complementary** error function (Abramowitz and Stegun, 1965, p.297), t is the time coordinate, y the depth coordinate, κ the thermal diffusivity for the lithosphere, T_s the surface temperature, and T_m the mantle (**asthenosphere**) temperature. As seen in Fig. 6c, we can look at this one-dimensional heating problem with thinning of the lithosphere as being the reverse of the cooling and thickening of the ocean lithosphere on Earth by conductive cooling of a semi-infinite half space solid (Turcotte and Oxburgh, 1969). For our problem, a linear equation of state is assumed, of the form:

$$\rho - \rho_m = \alpha \rho_m (T_m - T) \quad (24)$$

where α is the volume coefficient of thermal expansion, and ρ the density in the lithosphere corresponding to a temperature T . One can then express the w parameter

shown in Fig. 6C (analogous to the thermal subsidence in the case of the cooling problem) using the condition of HE of Eq. (15). Indeed, substitution of the temperature profile of Eq. (23) into Eq. (24) and then substituting the result in Eq. (15) yields (Turcotte and McAdoo, 1979):

$$w = 2\alpha (T_m - T_s) \left(\frac{\kappa t}{\pi}\right)^{1/2} \quad (25)$$

For the lithospheric temperature distribution given in Eq. (23) we can then give an (arbitrary) definition of the thermal lithosphere thickness Y_L . Indeed, a reasonable choice is (Turcotte and McAdoo, 1979, Turcotte and Schubert, 1982: $T_m - T = 0.1 (T_m - T_s)$ at $y = Y_L(t)$). Thus the thinned thermal lithosphere, as a thermal boundary layer (Turcotte and Schubert, 1982), is the near surface region where there is a significant temperature change. Using Eq. (23) and our definition of the thermal lithosphere thickness we can then express Y_L as a function of t :

$$Y_L(t) = 2 (\kappa t)^{1/2} \operatorname{erfc}^{-1}(0.1) = 2.32 (\kappa t)^{1/2} \quad (26)$$

That is the thickness of the thermal boundary layer is 2.32 times the characteristic thermal diffusion distance $(\kappa t)^{1/2}$. Then, using Eq. (26) to eliminate t in Eq. (23), the temperature profile in the lithosphere can be written in terms of the dependent variable y , as:

$$\frac{T_m - T}{T_m - T_s} = \operatorname{erfc}\left(1.16 \frac{y}{Y_L}\right) \quad (27)$$

Similarly, the corresponding value of w can be written from Eq. (25) as:

$$w = \frac{2\alpha (T_m - T_s)}{2.32 \sqrt{\pi}} Y_L \quad (28)$$

A reference state is defined as corresponding to the unperturbed lithosphere, that is the situation when the lithosphere has not yet experienced basal heating and thinning. We will note as y_{L_0} the thickness of the lithosphere in the reference state, corresponding to zero thermal elevation (ie $h^{th} = 0$) with respect to the reference sphere (radius $R_0 = MPR = 6051.839$ km). With w_0 the corresponding reference state value of w , we then have (as seen in Fig. 6c):

$$h^{th} = w_0 - w = 0.486a (T_m - T_s)(y_{L_0} - y_L) \quad (29)$$

with y_L the thickness of the thinned lithosphere, corresponding to an elevation of h^{th} , and $y_{L_0} - y_L$ representing the thickness of lower lithosphere which is now asthenosphere at $T = T_m$. Note that we have $w_0 = h_{max}^{th}$, with h_{max}^{th} defined as the maximum thermal elevation (uplift) attainable, and corresponding to a totally thinned lithosphere (ie $y_L = 0$).

We can then use Eq. (16) (HOT formula) along with the equation of state Eq. (24) and the expression for the temperature distribution in Eq. (27) to obtain the geoid anomaly N_{th} corresponding to a surface elevation of h fully compensated by thermal thinning of the underlying lithosphere. With respect to the reference state defined above, the local geoid anomaly for this situation is given by:

$$N_{th} = - \frac{2 \pi G \rho_m \alpha (T_m - T_s)}{g_0} \left[1 + \frac{2\alpha (T_m - T_s)}{\pi} \frac{(y_L^2 - y_{L_0}^2)}{(2.32)^2} \right] \quad (30)$$

Using Eq. (28), Eq. (30) can be re-written as:

$$N_{th} = \frac{\pi G \rho_m}{g_0} \cdot \left[1 + \frac{\pi}{2\alpha (T_m - T_s)} \right] (w_0^2 - w^2) \quad (31)$$

And, with $h = w_o - w$ and $W. + w = 2 w_o - h$, Eq. (31) finally yields:

$$N_{th} = \frac{\pi G \rho_m}{g_o} [1 + 2\alpha \frac{\pi}{(T_m - T_s)}] (2 w_o h - h^2) \quad (32)$$

which is a quadratic function of elevation h as was the Airy compensation model formula. For the parameters of the thermal compensation model applied to the Venus data we took: $a = 3 \times 10^{-5} \text{ K}^{-1}$ and $\kappa = 1 \text{ mm}^2 \text{ s}^{-1}$ as for the Earth, and $T_s = 750^\circ \text{K}$, $T_m = 1500^\circ \text{K}$, and $\rho_m = 3300 \text{ kg m}^{-3}$ (Turcotte, 1993).

V. REGIONAL CORRELATIONS: **RESULTS** AND DISCUSSION

Using selection criteria based on tectonic style, regional morphology and gravity characteristics Solomon et al (1992) divide the Venus highlands into three basic classes. Representatives from two of these classes, namely broad topographic swells (or “volcanic rises”) and plateau - shaped highlands, can be found in the equatorial zone on Venus. In this section, we consider and discuss correlations for sets of averaged data points for observed topography, gravity, and geoid anomalies as well as gravity from the uncompensated topography for five sample regions located in the Venusian equatorial highlands and including representatives from both the swell-type and plateau-shaped morphologies. One sample is in Beta Regio and the other four in Aphrodite Terra, the largest highland area on Venus. This continent-sized region straddles the equator from $-45^\circ \text{E} < \text{longitude} < 210^\circ \text{E}$ and encompasses a variety of terrains. The changing physiography across its length makes it straightforward to divide Aphrodite into four well defined areas including, from West to East (Solomon et al., 1992): **Ovda** and **Thetis** **Regiones**, a central **Chasmata** area and the Easternmost **Atla Regio**.

For each of these five regions we selected a $30^\circ \times 30^\circ$ area to examine the regional h , N data correlations in the light of the three isostasy models discussed in Section IV. The chosen areas are outlined by black squares in Fig. 1a and 1 b. For our

Beta Regio sample we have: $-90^\circ < \text{longitude} < -60^\circ$, and $10^\circ < \text{latitude} < 40^\circ$. Beta is an example from the broad topographic rise category. It is a **domal** structure, approximately 3000 km across, with heights reaching -2-3 km above the mean **planetary** radius (MPR) from center to edge of the structure (Bindschadler et al., 1992b). It is also a region of moderate extensional deformation but has extensive shield volcanism (Senske et al., 1992). The topographic peaks of Beta, believed to be volcanoes, include Rhea Mons to the North (peaking at -5.5 km above MPR) in a region of **tessera** terrain, and Theia Mons, to the South, a shield-shaped structure peaking at -4 km above MPR. Both show evidence of collapse (Ford and Pettengill, 1992). Running approximately North-South in Beta Regio is **Devana Chasma**, a major trough (-1-to-2 km deep) believed to be a rift valley (McGill et al., 1981; Solomon et al., 1992).

The **Ovda** sample ($75^\circ < \text{longitude} < 105^\circ$, and $-20^\circ < \text{latitude} < 10^\circ$), and the Thetis sample ($110^\circ < \text{longitude} < 140^\circ$, and $-25^\circ < \text{latitude} < 5^\circ$) are typical examples from the topographic plateau class of highlands. They are characterized by highly deformed and complex ridged terrain (often interpreted as products of **crustal** shortening) and limited volcanism, with mean elevations of -4 km above the MPR (Solomon et al., 1992; Bindschadler et al., 1992b). Both these regions have rugged terrain over a wide range of horizontal scales. This was analyzed earlier in more details for **Ovda Regio** in terms of roughness amplitudes and fractal behavior for $36 \leq \lambda \leq 703$ km (Kucinskis et al., 1992). Unlike Ovda, Thetis Regio has less steep margins. Also, the highest points of Thetis are found along the area's margins with a noticeable offset of the positive geoid and topography anomaly highs (Bindschadler et al., 1992b). Our central Aphrodite sample ($145^\circ < \text{longitude} < 175^\circ$, and $-25^\circ < \text{latitude} < 5^\circ$) is part of a highly deformed "Chasmata area" which is in a class of its own. The region has mean elevations of only 1-1.5 km above MPR and presents a series of elongated ridges and linear to **arcuate** troughs (Ford and Pettengill, 1992; Solomon et al., 1992). The deepest troughs are Diana and Dali Chasmata. Finally, we considered a sample in **Atla Regio** ($180^\circ < \text{longitude} < 210^\circ$, and

-1 5° < latitude < +15°). This is another example of Beta-type topography (ie a broad highland dome), with mean elevations of 2-4 km above MPR, extensional features and numerous volcanic centers (Solomon et al., 1992). The two main **peaks** in Atla are the shield volcanoes Ozza Mons (6 km) to **the** Northeast, and Maat Mons (9 km) in the central part. Overall, Atla is mom strongly peaked and less circular in shape than Beta **Regio**.

For each of the 30° x 30° areas we considered in this work we determined mean values over 5° x 5° grid squares of observed topography anomaly $h = R - R_0$, and geoid anomaly N using Eqs. (1) and (5) and the spherical harmonic models for Venus data discussed in Section II, respectively. We also obtained 5° x 5° data values in each selected area of observed gravity anomaly Δg , using Eq. (8), and of the **Bouguer** gravity Δg^u and **Bouguer** gravity anomaly $BA = A g^u - A g$, where $A g^u$ is the gravity corresponding to the uncompensated topography and is obtained by replacing $\Delta \bar{C}_{lm}$ and $\Delta \bar{S}_{lm}$ in Eq. (8) by C_{lm}^u and S_{lm}^u of Eq. (14).

For a given sample region we first performed a linear least squares fit for the 5° x 5° data values of BA plotted against Δg^u . We define the regional degree of compensation C (Turcotte et al., 1981) as the slope of the best fit regression line for the considered data. We then performed a least squares fit of the observed geoid anomaly N versus elevation h regional data points to the Pratt, Airy, and thermal correlation models respectively. For each sample area, fitting of the three isostasy models to the h , N data yields values for the following model parameters: the regional GTR (in m/km) or the slope of the best fitting correlation line and the corresponding regional depth of compensation W (km) from Eq. (20) for the Pratt mechanism. For the Airy correlation: the zero-elevation **crustal** thickness H (km) and, for a given maximum regional elevation h_{max} , the corresponding total **crustal** thickness $T(h_{max}) = H + b(h_{max})$ with b the Airy root from Eq. (21). In this paper, h_{max} is defined as the maximum amplitude for the topography on a regional scale, with $\lambda = 3000$ km for our samples. Finally, for the thermal thinning

model, the thickness y_{L_0} of the unperturbed (zero-elevation) thermal lithosphere, obtained from the best fit regional parameter W . ~~h_{max}th~~ using Eq. (28). From section IV subsection c, we recall that h_{max}^{th} is the maximum elevation attainable with the thermal thinning model for the observed data in the considered area and corresponds to $y_L = 0$. For each sample area and for a maximum observed regional elevation h_{max} we also evaluate the corresponding thickness of the thinned lithosphere $y_L(h_{max})$, if applicable, using Eq. (29). For all considered areas a goodness of fit test (**chi-square**) was performed to assess how close the h, N data is to a linear Pratt model correlation and a quadratic Airy or thermal model correlation, respectively. A measure of the goodness of fit is given in each case considered by this statistic or root mean squared error (rinse) for the modeled data points (Milton and Arnold, 1986): $s = (\chi^2 / v)^{1/2}$, with χ^2 the minimized **chi-square** merit function and $v = n - p =$ the number of degrees of freedom of the problem, p being the number of free parameters of the considered **model** ($p = 2$ for the linear correlation and $p=3$ for the quadratic correlations), and $n = 36$ for all five regions considered in this study. Results of the various fits are given in Table II.

In Fig. 7 we show scatter plots of BA versus Δg^u for 36 $5^\circ \times 5^\circ$ data points (shown as open circles) in each of our five chosen areas. From the results of the degree of compensation fits shown in Table II it can be seen that C is high for all the considered highland regions. However, compensation of these equatorial highlands seems particularly significant in the high - plateaus (with Ovda and Thetis 89% compensated) while the swell-type areas appear to be less compensated. Fig. 8 shows scatter plots of N versus h (open circles) for the 36 observed data points in our regions of interest. The best fit correlation for the Pratt, Airy, and thermal thinning models are shown as solid curves in Fig. 8a, 8b, and 8c respectively. Overall, we note that for each area regional h, N data correlations display strong coherence. However, from Table II we see that for all three models considered there are large variations in model parameters between the regional fits. Another trend readily apparent from the scatter plots in Fig. 8 is the

positive **geoid** offset observed at the regional level (ie N non zero for zero elevation h in some areas). This offset or regional anomaly is large for Atla and Thetis **Regiones** and the **Chasmata** area but negligible in Beta and **Ovda**. In what follows we discuss results of fits of each of the three theoretical correlations to the regional h , N data,

From Table II we can see that for the Pratt regional correlations there is a definite grouping into classes based on values of GTR and associated depth of compensation W . Indeed, these parameters are largest for the topographic swells of Beta and Atla **Regiones** while the **Ovda** and Thetis **Regiones** plateaus have smaller Pratt parameter values. The **Chasmata** area sample has somewhat intermediate values. These observations suggest the applicability of different mechanisms of compensation for different classes of equatorial regions on Venus. This seems particularly true for Aphrodite Terra, where the numbers in Table II show a significant increase in regional GTR and W from the west to east. The numerical values we obtained here for regional GTR and the tendency to categorize the Venus equatorial highlands based on regional correlations of geoid and topography data confirm for the **Magellan** data results of previous investigations conducted with lower resolution PVO data (Herrick et al. 1989; Black et al, 1991; Smrekar and Phillips, 1991).

If we assume isostatic compensation mechanisms for the equatorial highlands on Venus then there is a similarity between the results obtained in this work for the Beta, Atla, and **Chasmata** area h , N data in terms of Pratt linear correlation and results obtained for oceanic swells on the Earth (eg the Hawaiian swell). Physical mechanisms which have been invoked to explain observed correlations of Earth geoid and depth (bathymetry) variations in these types of oceanic regions include anomalously low densities of mantle rocks beneath the swells to depths of W (Haxby and Turcotte, 1978), and thermal lithospheric thinning (Crough, 1978; Turcotte, 1986). The **Ovda** and Thetis group's linear correlation results are similar to those obtained for ocean plateaus on Earth (Turcotte, 1986). Thickening of the crust is often invoked as a compensation mechanism

for these terrestrial oceanic features (Crough, 1978; Sandwell and MacKenzie, 1989; Marks and Sandwell, 1991).

For the Airy compensation model correlations the best fit parameter values for H show the same regional tendencies as the Pratt model's GTR and W parameters, with a West to East increase in H in Aphrodite Terra. For Ovda Regio ($H \sim 50$ km) and Thetis Regio ($H \sim 60$ km), the zero-elevation crustal thickness seems realistic if one envisages a thick thermal lithosphere on Venus. The value of H for the Chasmata area sample could be considered, although at $H \sim 100$ km it is probably already a little too high, even with a thick lithosphere. If isostasy is to be considered here, we probably have to consider a mix of Airy-compensated crustal thickening with another model's component. For the two other regions we considered, namely Beta and Atla Regiones regional H values required to account for elevations typically found in those areas are probably unrealistic ($H > 150$ km) even if a very thick lithosphere is envisaged. If there is Airy compensation there, it is probably a weaker component in a mix of other mechanisms.

In the case of the thermal correlations it must first be noted (Fig. 8c and Table 11) that the lithospheric thinning model barely manages to reproduce the Thetis Regio data, with $h_{\max}^{\text{th}} = 3.0$ km compared to the observed value of $h_{\max} = 3.6$ km for the considered region. This is an inclination that the thermal model alone is probably inadequate for fully explaining the observed data in Thetis. Also, the thermal model badly fails for the Ovda Regio data, with $h_{\max}^{\text{th}} = 2.7$ km much less than the observed $h_{\max} = 4.0$ km. Clearly, if there is a thermal isostasy component in Ovda it must be very weak. For the other three regions we considered a thermal thinning model can account for the observed topography and geoid anomaly data. However, it seems reasonable to assume that it is quite possible there are variations in the thermal component's strength even between those higher GTR regions. In any case, if the thermal model is to

reproduce the observable in those areas, a thick zero-elevation thermal lithosphere is required of the order of 300 km.

From the preceding results it thus appears that the geoid - topography correlations observed in the Venus equatorial highlands considered in this work can be reproduced, as is the case on the Earth, by isostatic compensation mechanisms involving (and quite possibly combining) variations in **crustal** thickness (Airy compensation) and variations in thermal lithosphere thickness (thermal thinning) provided a thick crust and unperturbed thermal lithosphere are **assumed** on Venus, with zero-elevation thermal lithospheric thickness y_{L_0} of about 300 km. One recent model proposed to obtain a thick Venusian lithosphere is **Turcotte's** (1993) episodic hypothesis for tectonics on Venus. **Turcotte** supposes that loss of heat from the interior of Venus is strongly time - dependent (ie non steady-state). Indeed, crater statistics on Venus strongly suggest that a global resurfacing event occurred on the planet -500 ± 300 My before present (BP) and that the global lithosphere on Venus later stabilized (**Schaber et al., 1992 a, b**). Thus **Turcotte** postulated that the global lithosphere on Venus, after stabilizing some 500 My BP has since then been a single rigid lithospheric plate that has thickened due to conductive cooling. A straightforward calculation then yields a thermal lithospheric thickness of ~ 300 km reached after some 500 My.

Based on the above premises, modes of isostatic compensation could be distributed among the highland areas considered in this study as follows: for the low GTR area in Ovda and Thetis Regiones, we would favor mainly Airy compensated crustal thickening with a zero-elevation crustal thickness of around 50- 60 km. For our Chasmata area sample, we would consider Airy isostasy with perhaps a thermal component. Finally, for the large GTR areas of Beta and Atla Regiones, a very strong thermal compensation component. indeed, the very large values of H obtained for these two regions are unrealistic even with a 300 km thick thermal lithosphere. It is also interesting to try and explain the Eastward increase in Regional Pratt and Airy model

parameters observed across the length of Aphrodite Terra. A possible explanation of this phenomenon could be that Aphrodite is a site of thermal isostasy decay, experienced from East to West. Indeed, Herrick et al. (1989) suggested that the Eastward increase in depths of compensation in Aphrodite reflects an age progression for underlying mantle plumes responsible for maintaining (dynamically in their analysis) topography highs in this area. To the East would be younger, more vigorous, plumes while older decaying plumes would be located in the West. In the context of our isostatic approach to compensation of Venusian highlands we suggest there may very well be such a correlation between Airy and Pratt model parameters and mantle plume age/strength operating East of **Ovda Regio**. However, temporal decay of plume strength from the east to the west beneath Aphrodite would be associated with a decaying thermal thinning compensation of surface topographic swells. Thermal isostasy decay was proposed by **Sandwell** and **MacKenzie** (1989) as an explanation for intermediate GTR values observed for **certain** thermally older oceanic swells on the Earth, in association with an Airy isostasy component.

v]. CONCLUSIONS

In this paper we have taken an isostatic approach to study the compensation mechanism in five $30^\circ \times 30^\circ$ areas characteristic of the main classes of highlands found in the equatorial zone on Venus. Gridded mean values of Bouguer gravity and observed gravity, geoid and topography anomalies were obtained for each area using a 120×120 degree and order spherical harmonic model for the Venusian global topography produced using **Magellan** and PVO altimetry data and a 60×60 harmonic solution for the Venus geopotential which incorporates new tracking data from the **Magellan** circularized orbit (cycle 5) as well as previous **Magellan** cycle 4 and PVO tracking data.

A 'global spectral study conducted on these harmonic models reveals that their power spectral density obey a power-law scaling. The Venus topography spectrum has the characteristics of Brown noise (spectral slope $\beta - 2$) similar to Earth topography but with lower amplitudes, and a slightly shallower spectral slope, a possible consequence of

the dominant "rolling plains" Venusian topography. The spectral slope for the Venus geoid spectrum is close to the value predicted by Kaula's law ($\beta - 3$) which applies to the Earth's geoid spectrum. A degree analysis of the GTR for the harmonic models further shows that Venusian topography is substantially compensated. If a global Airy compensation is assumed then most of the topography on Venus is compensated at depths in excess of 100 km implying a thick crust and lithosphere.

For the regional study in this paper three types of models were considered to test the 36 geoid versus topography anomaly data points in each of the chosen areas for theoretical isostasy correlations: Pratt and Airy isostatic compensation mechanisms, and a thermal isostasy model with support of the topography obtained via thinning of the thermal lithosphere by reheating. We also examined linear correlations of Bouguer anomaly versus Bouguer gravity to estimate regional degrees of compensation.

In all five regions we analyzed the h , N data generally showed little scatter. For the plateau - shaped areas of Ovda and Thetis *Regiones* compensation was the highest. Ovda and Thetis *Regiones* feature the lowest values for geoid to topography ratio, Pratt depth of compensation, and Airy zero-elevation crustal thickness ($H \sim 50$ and 60 km respective y) among the samples we considered. For the Chasmata area values for these parameters are somewhat higher with $H \sim 100$ km. The thermal thinning model barely manages to account for observed elevations in Thetis and fails to reproduce most of Ovda's high topography. It is thus suggested that Airy compensation with a thick crust and lithosphere is the dominant support mechanism for topography in Ovda and Thetis whereas a higher value of H for the Chasmata sample might indicate a mix of Airy and thermal components in this area,

The topographic swells of Beta and Atla *Regiones* have somewhat lower degrees of compensation. Pratt and Airy model parameter values estimated for these regions are significantly larger than for the plateau class topographies. In particular, Airy regional crustal thicknesses seem unreasonably large ($H \sim 200$ km) even if a thick lithosphere is

assumed. The thermal **isostasy** model **easily** accounts for the observed topography and **geoid** anomaly data in these regions but requires thinning of an initially thick (-300 km) thermal lithosphere. This suggests that thermal thinning is the dominant component for **isostatic** compensation **in** these two areas.

Four of our samples were chosen in Aphrodite Terra namely, from West to East: **Ovda**, Thetis, the central **Chasmata** area, and Atla to the East. Results for these areas shown a significant Eastward increase of Pratt and Airy model parameter values for this continent. We propose that this phenomenon might be attributed to a decay in mantle plumes responsible for reheating and thinning of the lower lithosphere from the East to the West in Aphrodite.

On the Earth, most of ~~the~~ high topography can be directly associated with variations in **crustal** (Airy compensation) and/or **lithospheric** (thermal isostasy) thicknesses. The present study indicates this may also be the case for the Venus equatorial highlands provided Venus has a thick unperturbed thermal lithosphere with thickness of about 300 km. One way to account for such a thick lithosphere would be conductive cooling during the past - 500 My, as suggested by Turcotte (1993). In future investigations we will conduct a systematic analysis of compensation for the Venus highlands from an **isostatic** standpoint, implementing and developing the technique introduced in the present work. The quantitative analysis of gravity data covering the entire planet should be greatly improved once **geopotential** models incorporating the complete circular orbit tracking data become available.

ACKNOWLEDGMENTS

This research has been supported by the National Aeronautics and Space Administration under grants **JPL 958935** and **NAGW- 1420**. We wish to thank **Nicole Rappaport** for her contributions and friendly advice which were of great value during the completion of this work at JPL. Our many thanks to **Bill Sjogren** and **Alex Konopliv** for

making the **Magellan** data available to us and for helpful criticism, to the Navigation team of section 314 at JPL for their support, to Richard Rapp at **the** Ohio State University for providing us with his harmonic model for **Earth** topography, and Bob Williams at **JPL** for the Topex /Poseidon Earth gravity model. We also greatly benefited from discussions with George **Balmino** and Jean-Pierre Barnot of the CNES, and **Dah-Ning** Yuan at JPL. Department of Geological Sciences, Cornell University, contribution number 870.

REFERENCES

- Abramowitz, M., and I. A. Stegun 1965. *Handbook of Mathematical Functions*, Dover, New York.
- Balmino, G. 1986. Present status and future improvements in measuring the gravity field of the Earth and Planets. In *Space Geodesy and Geodynamics*, edited by A. J. Anderson and A. Cazenave, Academic Press, London.
- Balmino, G., K. Lambeck, and W. M. Kaula 1973. A spherical harmonic analysis of the Earth's topography. *J. Geophys. Res.* **78**, No. 2, 478-481.
- Bills, B. G., W. S. Kiefer, and R. L. Jones 1987. Venus gravity: A harmonic analysis. *J. Geophys. Res.* **92**, 10335-1W51.
- Bindschadler, D. L., A. De Charon, K. K. Beratan, S. E. Smrekar, and J. W. Head 1992a. Magellan observations of Alpha Regio: Implications for formation of complex ridged terrains on Venus. *J. Geophys. Res.* **97**, 13563-13577.
- Bindschadler, D. L., G. Schubert, and W. M. Kaula 1992b. Coldspots and hotspots: Global tectonics and mantle dynamics on Venus. *J. Geophys. Res.* **97**, 13495-13532.
- Black, M. T., M. T. Zuber, and D. C. McAdoo 1991. Comparison of observed and predicted gravity profiles over Aphrodite Terra, Venus. *J. Geophys. Res.* **96**, No. B1, 301-315.

- Crough, S. T. 1978. Thermal origin of mid-plate hot-spot swells. *Geophys. J. R. astr. Soc.* 55,451-469.
- Dahlen, F. A. 1982. Isostatic geoid anomalies of a sphere. *J. Geophys. Res.* 87, 3943-3947.
- Ford, P. G., and G. H. Pettengill 1992. Venus topography and kilometer-scale slopes. *J. Geophys. Res.* 97, E8, 13103-13114.
- Hager, B. H. 1983. Global isostatic geoid anomalies for plate and boundary layer models of the lithosphere. *Earth Planet. Sci. Lett.* 63, 97-109.
- Haxby, W. F. and D. L. Turcotte 1978. On isostatic geoid anomalies. *J. Geophys. Res.* 83, No. B 11, 5473-5478.
- Heiskanen, W. A., and H. Moritz 1967. *Physical Geodesy*, W. H. Freeman, San Francisco, California,
- Herrick, R. R., B. G. Bills, and S. A. Hall 1989, Variations in effective compensation depth across Aphrodite Terra, Venus. *Geophys. Res. Lett.* 16, No. 6,543--546.
- Kaula, W. M. 1977. Geophysical inferences from statistical analysis of the gravity field. *Dep. Geod. Sci. Rep.* 250, pp. 199-141, Ohio State Univ., Columbus.
- Kaula, W. M. 1984. Tectonic contrasts between Venus and the Earth. *Geophys. Res. Lett.* 11, No. 1, 35-37.

- Kiefer, W. S., and B. H. Hager 1991. A mantle plume model for the equatorial highlands of Venus. *J. Geophys. Res.* 96,20947--20966.
- Konopliv, A. S., and W. L. Sjogren 1994. Venus spherical harmonic gravity model to degree and order 60. *Icarus*, this issue.
- Konopliv, A. S., N. J. Borderies, P. W. Chodas, E. J. Christensen, W. L. Sjogren, B. G. Williams, G. Balmino, and J. P. Barriot 1993. Venus gravity and topography: 60th degree and order model. *Geophys. Res. Lett.* 20, No. 21,2403-2405.
- Kucinskis, A. B., D. L. Turcotte, J. Huang, and P. G. Ford 1992. Fractal analysis of Venus topography in Tinatin Planitia and Ovda Regio. *J. Geophys. Res.* 97, No. E8, 13635-13641.
- Lambeck, K. 1976. Lateral density anomalies in the upper mantle. *J. Geophys. Res.*, 81, 6333-6340,
- Lambeck, K. 1988. *Geophysical Geodesy*, Clarendon Press, Oxford,
- Lliboutry, L. 1982. *Tectonophysique et géodynamique: Une synthese geologie structurale-geophysique interne*. Masson, Paris.
- Marks, K. M., and D. T. Sandwell 1991. Analysis of geoid height versus topography for oceanic plateaus and swells using nonbiased linear regression. *J. Geophys. Res.* 96, No. B5, 8045-8055.

- Masursky, H., E. Eliason, P. G. Ford, G. E. McGill, G. H. Pettengill, G. V. Schaber, and G. Schubert 1980. Pioneer Venus radar results: geology from images and altimetry, *J. Geophys. Res.* 85,8232-8260.
- McGill, G. E., J. L. Warner, M. C. Malin, R. E. Arvidson, E. Eliason, S. Nozette, and R. D. Reasenberg. 1983, Topography, surface properties and tectonic evolution, in *Venus*, edited by D. M. Hunten, L. Colin, T. M. Donahue, and V. I. Moroz, pp. 96-97. University of Arizona Press, Tucson.
- McGill, G. E., S. J. Steenstrup, C. Barton, and P. G. Ford 1981. Continental rifting and the origin of Beta Regio, Venus. *Geophys. Res. Lett.* 8,737-740.
- McNamee, J. B., N. J. Borderies, and W. L. Sjogren 1993. Venus: Global gravity and topography, *J. Geophys. Res.* 98, ES,911 3--9128.
- Milton, J. S., and J. C. Arnold 1986. *Probability and statistics in the engineering and computing sciences*. McGraw-Hill Book Company, New York.
- Morgan, P., and R. J. Phillips 1983. Hot spot heat transfer: its application to Venus and implications to Venus and Earth. *J. Geophys. Res.* 88, No. B 10, 8305-83 17.
- Moritz, H. 1980. *Advanced Physical Geodesy*, Abacus Press, Wells, Kent.
- Moyer, T. D. 1971. Mathematical formulation of the Double Precision Orbit Determination Program (DPODP). *Technical Report 32-1527* (internal document), Jet Propulsion Laboratory, California Institute of Technology, Pasadena, California.

- Nerem, R. S. et al. 1994. Gravity model development for Topex/Poseidon: Joint gravity models 1 and 2. *J. Geophys. Res.* (in press)
- Ockendon, J. R. and D. L. Turcotte 1977. On the gravitational potential and field anomalies due to thin mass layers. *Geophys. J. Roy. Astron. Soc.* 48,479-492.
- Pavlis, N. K., and R. H. Rapp 1990. The development of an isostatic gravitational model to degree 360 and its use in global gravity modeling. *Geophys. J. Int.* 100,369-378.
- Phillips, R. J. 1990. Convection-driven tectonics on Venus. *J. Geophys. Res.* 93, 1301-1316.
- Phillips, R. J., and M. C. Malin 1983. In *Venus*, edited by D. M. Hunten, L. Colin, T. M. Donahue, and V. I. Moroz, University of Arizona Press, Tucson.
- Phillips, R. J., W. L. Sjogren, E. A. Abbott, J. C. Smith, R. N. Wimberly, and C. A. Wagner 1979. Gravity field of Venus: A preliminary analysis. *Science* 205, 93-96.
- Phillips, R. J., W. M. Kaula, G. E. McGill, and M. C. Malin 1981. Tectonics and evolution of Venus. *Science*, 212, 879-887.
- Rapp, R. H. 1982. Degree variances of the Earth's potential, topography, and its isostatic compensation. *Bull. Geod.* 56, pp. 84--94.

Rapp, R. H. 1989. The decay of the spectrum of the gravitational potential and the topography for the Earth, *Geophys. J. Int.* 99,449-455.

Rappaport, N. J. 1994. Personal communication.

Rummel, R., R. H. Rapp, H. Sünkel, and C. C. Tscherning 1988. Comparisons of global topographic/isostatic models to the Earth's observed gravity field, *Report No.* 388, Department of Geodetic Science and Surveying, Ohio State University, Columbus.

Sandwell, D. T., and K. R. MacKenzie 1989. Geoid height versus topography for oceanic plateaus and swells. *J. Geophys. Res.* 94, No. B6, 7403–7418.

Schaber, G. G., H. J. Moore, R. G. Strom, and J. M. Boyce 1992a. The uniform distribution but non uniform modification of impact craters on Venus (abstract). *Lunar Planer. Sci., XXIII*, 1213--1214.

Schaber, G. G., R. G. Strom, H. J. Moore, L. A. Soderblom, R. L. Kirk, D. J. Chadwick, D. D. Dawson, L. R. Gaddis, J. M. Boyce, and J. Russell 1992b. Geology and distribution of impact craters on Venus: What are they telling us? *J. Geophys. Res.* 97, 13257–13301.

Senske, D. A., G. G. Schaber, and E. R. Stofan 1992. Regional topographic rises on Venus: geology of western Eistla Regio and comparison to Beta Regio and Atla Regio. *J. Geophys. Res.* 97, No. E8, 13395-13420.

- Sjogren, W. L., R. J. Phillips, P. W. Birkeland, and R. N. Wimberly 1980. Gravity anomalies on Venus. *J. Geophys. Res.* 85, 8295-8302.
- Smrekar, S. E., and R.J. Phillips 1991. Venusian highlands: geoid to topography ratios and their implications. *Earth and Planetary Science Letters* 107, 582-597.
- Solomon; S. C. et al. 1992. Venus tectonics: An overview of Magellan observations. *J. Geophys. Res.* 97, No, E8, 13199-13255.
- Surkov, Y. A., V. L. Barsukov, L. P. Moskalyeva, V. P. Kharyukova, and A. L. Kemurdzhian 1984. New data on the composition, structure, and properties of Venus rock obtained by Venera 13 and Venera 14. *J. Geophys. Res.* 89, B393-B402.
- Turcotte, D. L. 1980. On the thermal evolution of the Earth. *Planet. Sci. Lett.* 48, 53-58.
- Turcotte, D. L. 1986. Properties of the lithosphere and asthenosphere deduced from geoid observations. In *Space Geodesy and Geodynamics*, pp. 451-475, edited by A. J. Anderson and A. Cazenave, Academic Press, London.
- Turcotte, D. L. 1987. A fractal interpretation of topography and geoid spectra on the Earth, Moon, Venus, and Mars. *Proc. Lunar Planet. Sci. Conf. 17th, Part 2, J. Geophys. Res.* 92, suppl., E597-E601.
- Turcotte, D. L. 1989. A heat pipe mechanism for volcanism and tectonics on Venus. *J. Geophys. Res.* 94, No. B3, 2779-2785.

- Turcotte, D. L. 1993. An episodic hypothesis for Venusian tectonics. *J. Geophys. Res.* 98, 17061-17068.
- Turcotte, D. L., and G. Schubert 1982. *Geodynamics*, 450 pp., John Wiley, New York.
- Turcotte, D. L., and D. C. McAdoo 1979. Geoid anomalies and the thickness of the lithosphere. *J. Geophys. Res.* 84, No. B5, 2381-2387.
- Turcotte, D. L., R. J. Willemann, W. F. Haxby, and J. Norberry 1981. Role of membrane stresses in support of planetary topography. *J. Geophys. Res.* 86, No. B5, 3951-3959.
- Vening-Meinesz, F. A. 1951. A remarkable feature of the Earth's topography. *Proc. R. ned. Akad. Wet. B, Phys. Sci.*, 54, 212-228.
- Watts, A. B., and S. F. Daly 1981. Long wavelength gravity and topography anomalies. *Ann. Rev. Earth Planet. Sci.* 9, 415-448.
-

TABLE I
Results of Linear Fits for Planetary Spectra

Spectrum	Venus		Earth	
	κ	β	κ	β
Topography	-3.34	1.73	-4.03	2.08
Geoid	-1.80	2.91	-2.13	2.79

TABLE II
Parameters for Regional Model Fits

Region	h_{\max} km	CX100 %	GTR m/km	W km	'Pratt	H km	T km	$(h_{\max}) \sigma_{\text{Airy}}$	h_{\max}^{th} km	y_{L_0} km	$y_L(h_{\max})$ km	σ_{th}
Beta	2.8	52.1	31.9	409	16.5	223	244	16.4	4.0	369	113	17.5
Ovda	4.0	89.0	9.0	115	6.7	49.8	78.8	6.9	2.7	250	NA	11.1
'Thetis	3.6	89.7	11.3	144	12.8	65.7	91.8	12.9	3.0	275	NA	11.7
Chasmata	1. 2	79.9	15.1	194	7.1	107	115	7.2	1.8	165	55.0	6.7
Atla	3.0	63.8	24.9	319	12.0	167	189	12.1	4.0	362	88.0	12.6

FIGURE CAPTIONS

Figure 1: Contour maps of Venus in cylindrical equidistant projection. Negative contours are dashed, positive contours solid. (a) Topography variations above and below a spherical reference surface with radius $R_0 = 6051.839$ km and computed from a 120x 120 spherical harmonic model for Venus topography discussed in the text, truncated at degree and order 60. The contour interval is 500 m. (b) geoidal undulations computed from the 60 x 60 MGN P60FSAAP model for Venus geopotential described in the text. Geoid anomalies are measured with respect to a best fit sphere of radius R. and the contour interval is 10 m. The black boxes in Fig. 1a and Fig. 1b outline the equatorial areas analyzed in this paper.

Figure 2: Power spectral density of global observed topography for Venus (a) and the Earth (b), plotted against wave number on a log-log scale as open circles. The solid lines illustrate the best fit correlations with a power law with spectral slope $-\beta$.

Figure 3: Power spectral density (PSD) of observed global geoid anomaly for Venus (a) and the Earth (b) plotted against wave number on a log-log scale (open circle). The straight solid lines are the least-squares fits to a power law with spectral slope $-\beta$. in Fig. 3a, geoid PSD values corresponding to the biased MGNP60FSAAP solution are plotted as open circles whereas the unbiased solution PSD's are plotted as a dotted curve. The dashed curve in Fig. 3a is the geoid PSD for an Airy isostasy model for Venus topography

compensated at a depth of 150 km. In Fig. 3b the open circles correspond to data from the JGM-2 model for the Earth's **geopotential**.

Figure 4: Degree **geoid** to topography ratios (**GTR**) for Venus data plotted against degree ℓ on a log-linear scale. The open circles are for observed data and the solid curve is for an uncompensated topography model.

Figure 5: Degree **geoid** to topography ratios (**GTR**) for Venus plotted against degree P . The GTR for observed Venus data are plotted as open circles. The solid curves are degree GTR for Airy-type compensation models at depths of 50, 150, and 300 km.

Figure 6: Pratt - Hayford (a), Airy - Heiskanen (b), and thermal lithospheric thinning (c) models of **isostatic** compensation considered in this study.

Figure 7: Scatter plots of **Bouguer anomaly (BA)** versus **Bouguer gravity (Δg^u)** for the five equatorial regions considered in this paper. The open circles correspond to the data points. The solid lines are best fit linear correlations with the slope yielding a degree of compensation in each sample region considered (see text).

Figure 8: Scatter plots of **geoid anomaly (N)** versus **height anomaly (h)** for the five equatorial areas considered in this paper. Open circles are data points. Solid curves are best-fit theoretical correlations for the Pratt (a), Airy (b), and thermal thinning (c) models.

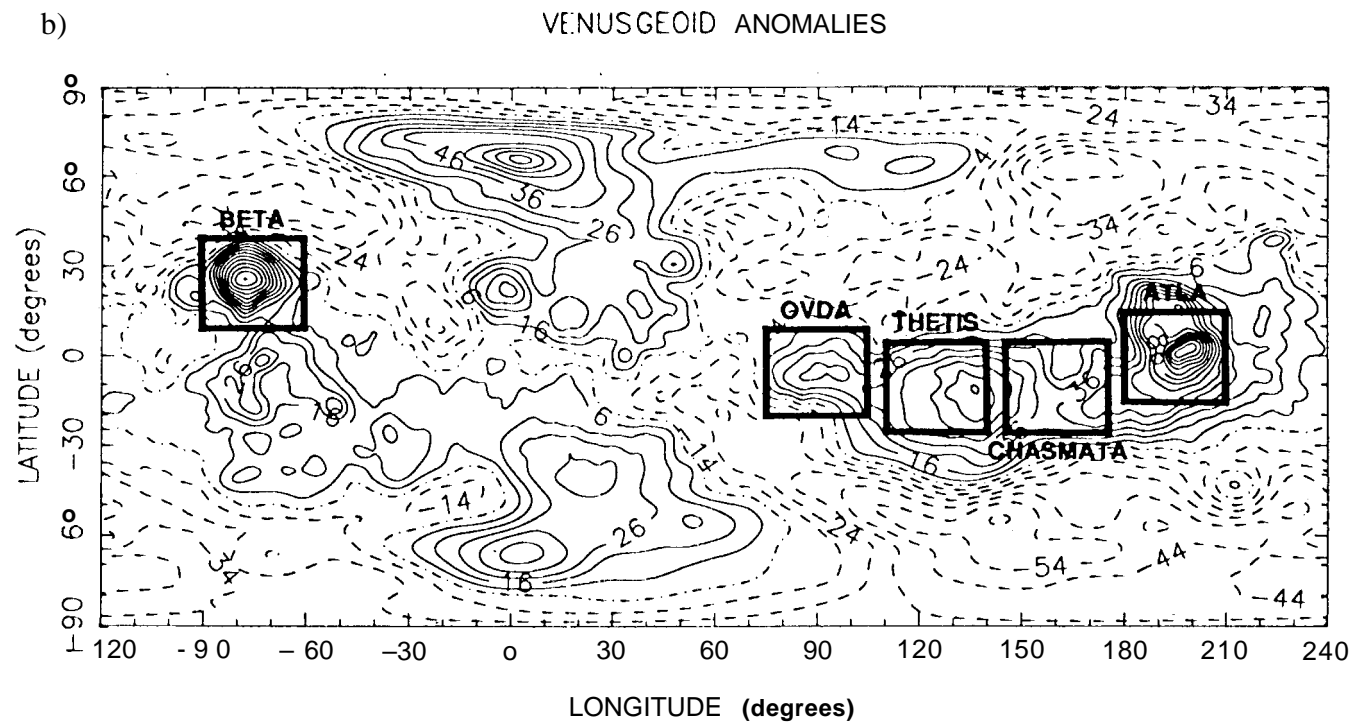
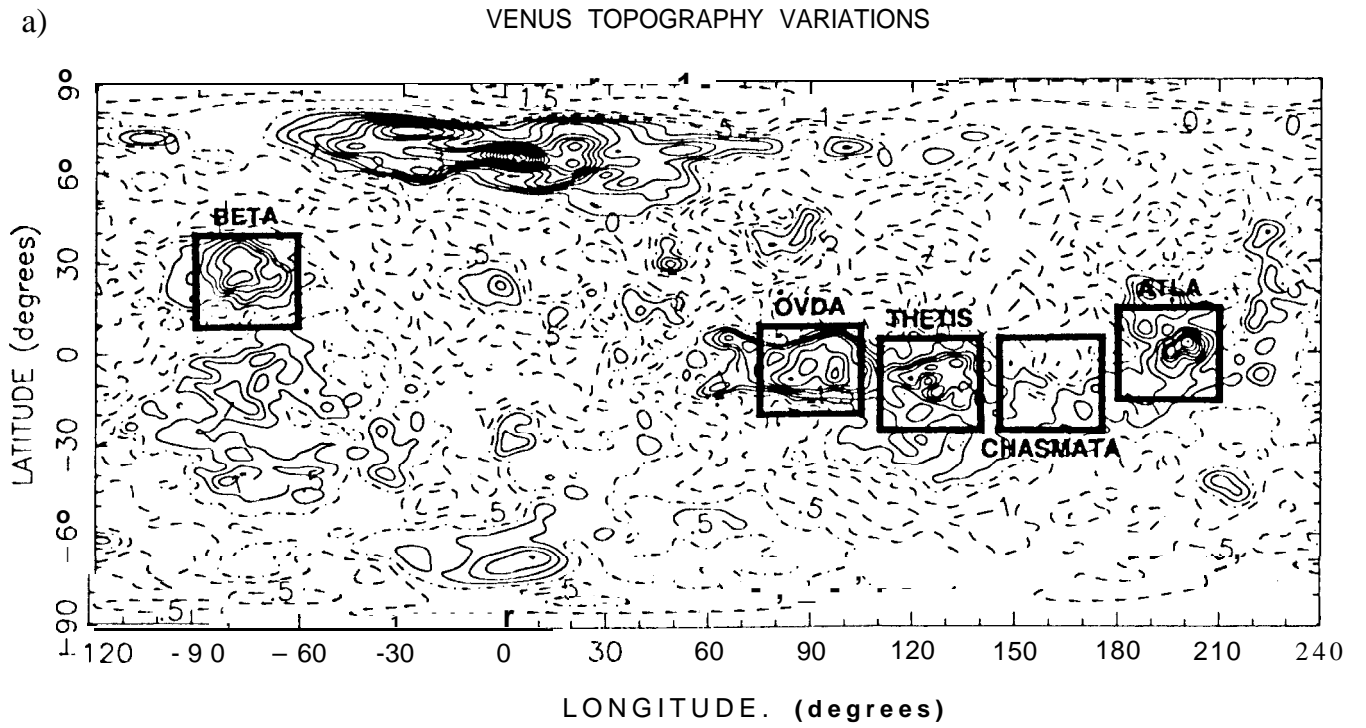
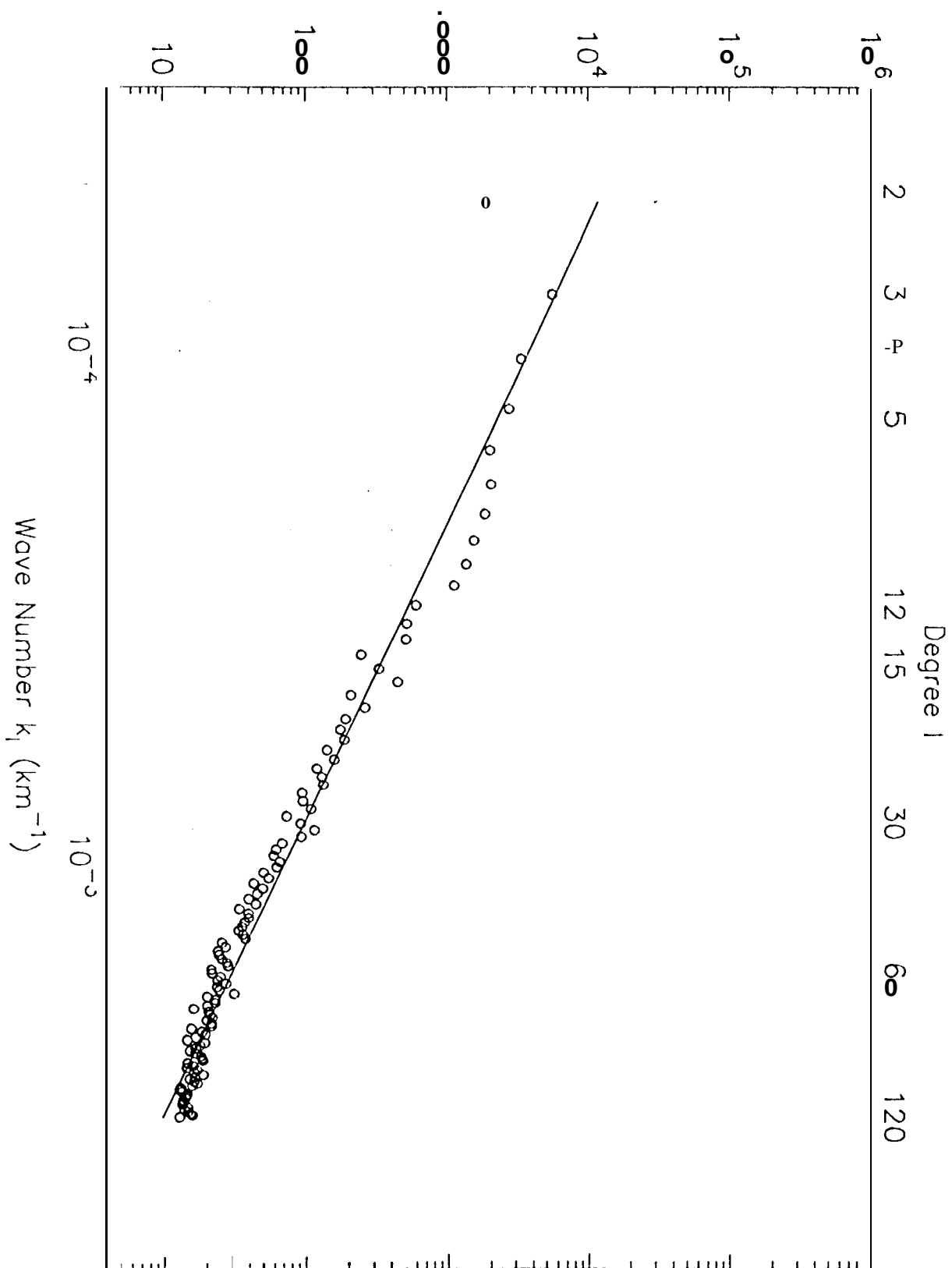


Fig. 1

a

Degree PSD for Venus Topography (km^3)



b

Degree PSD for Earth Topography (km^3)

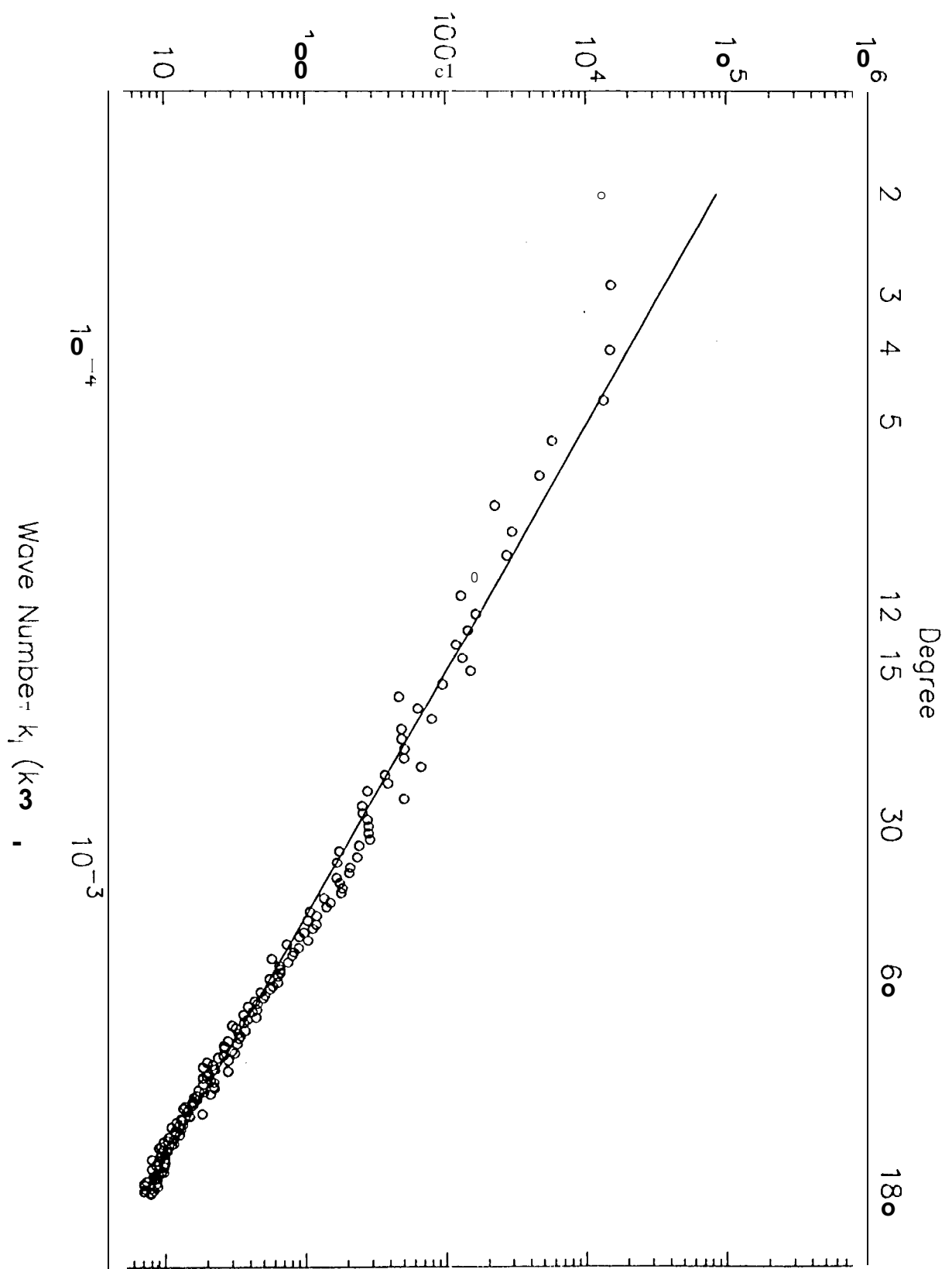


fig. 2b

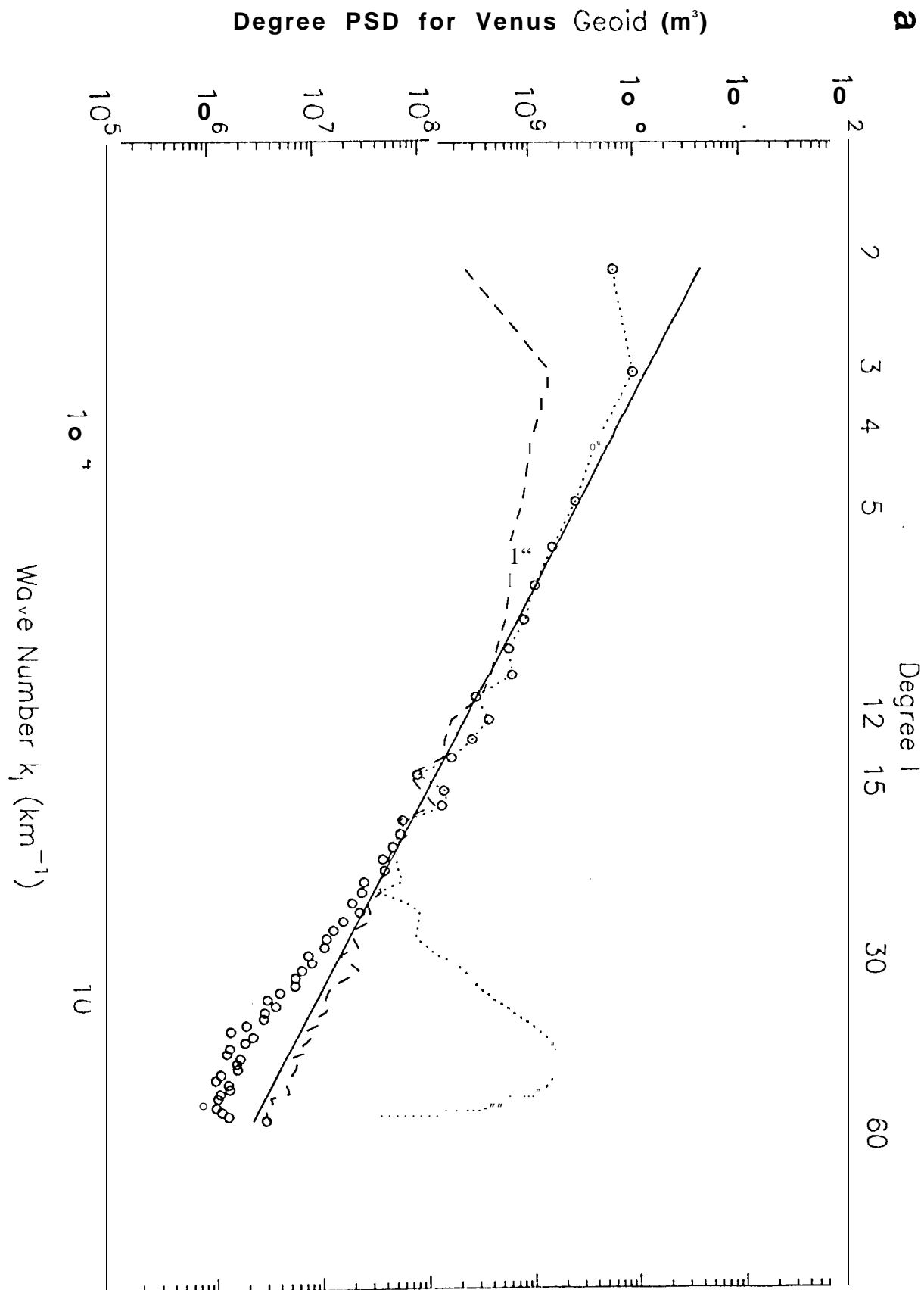


Fig. 3a

b

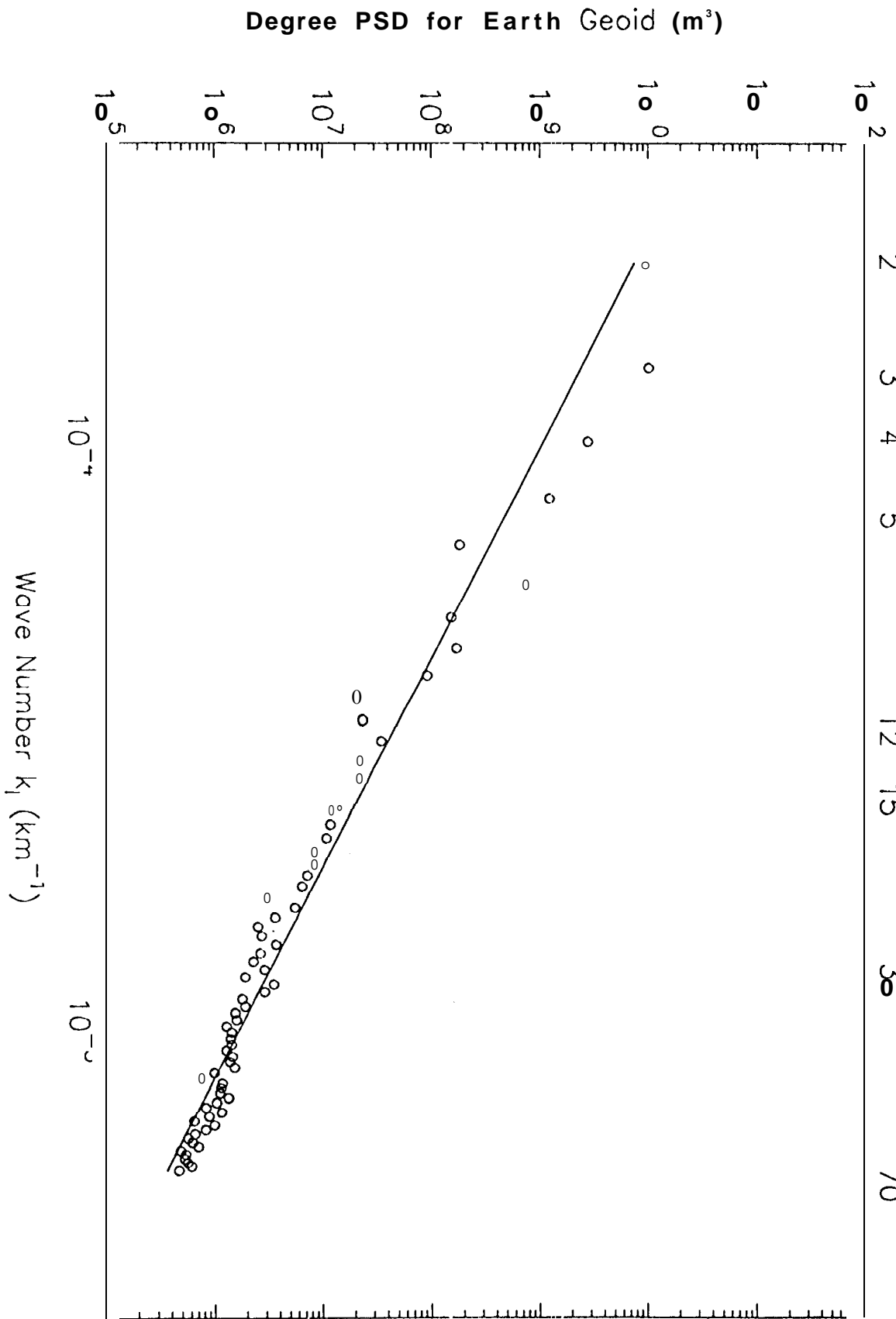


Fig. 3b

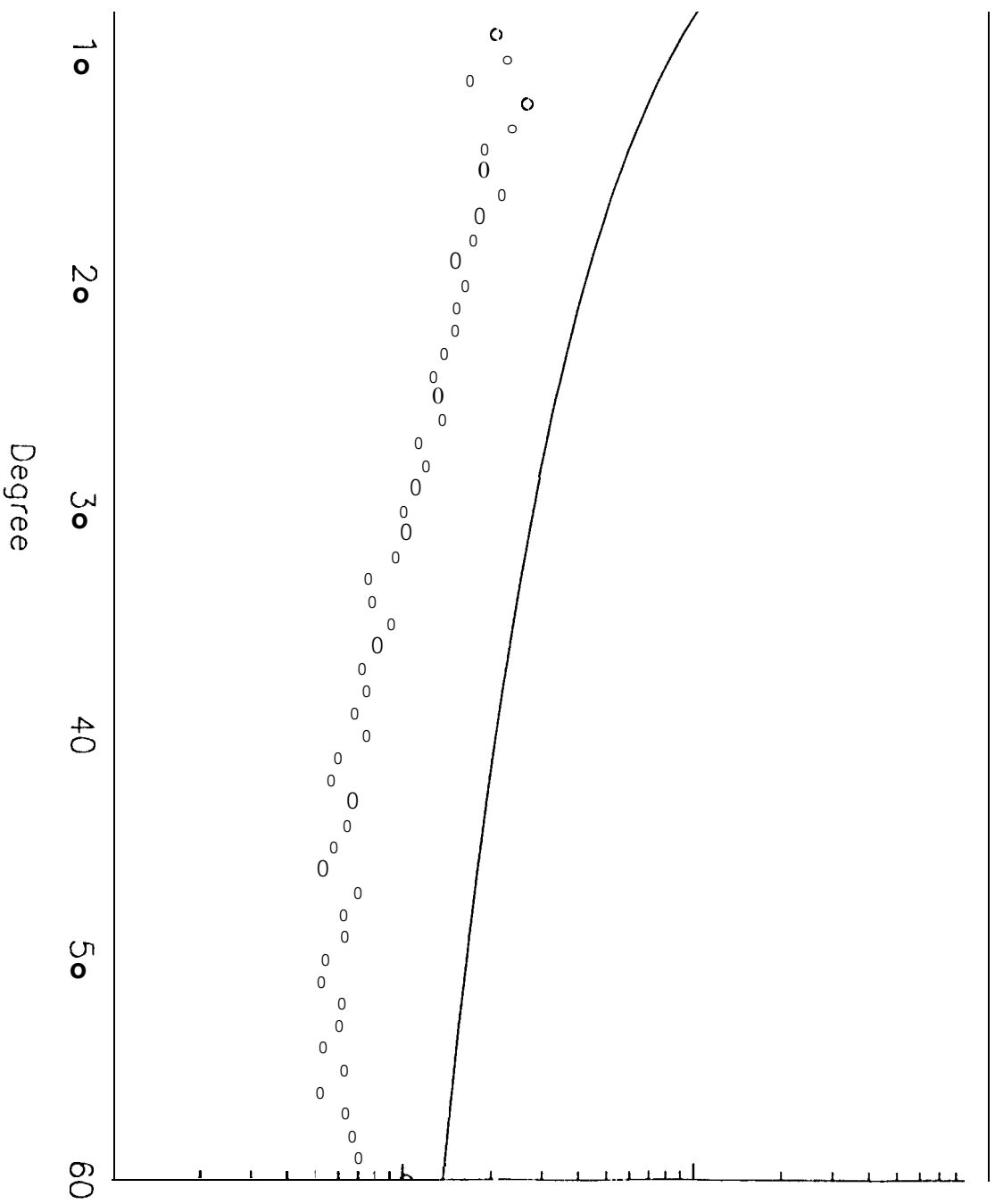
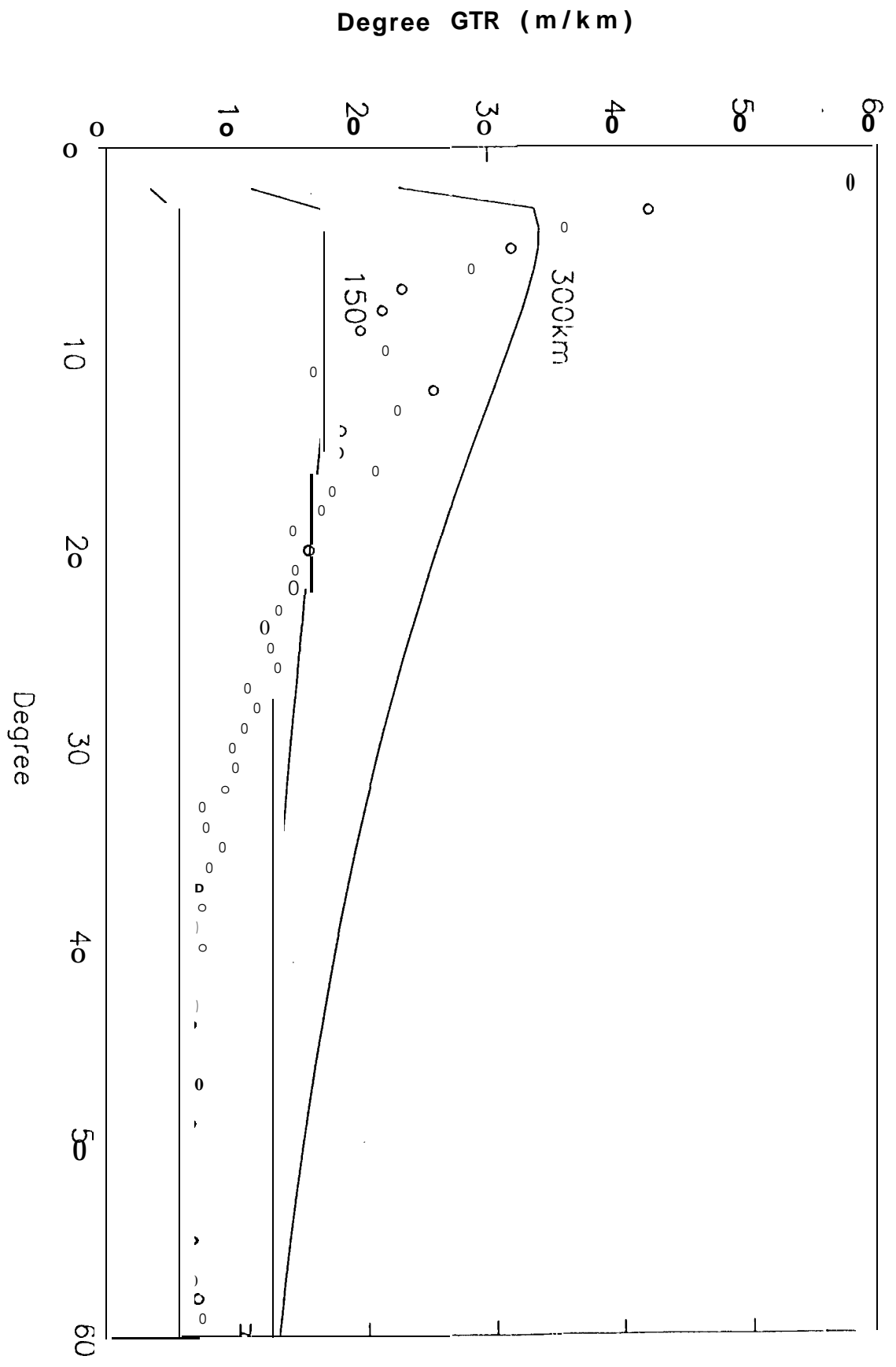
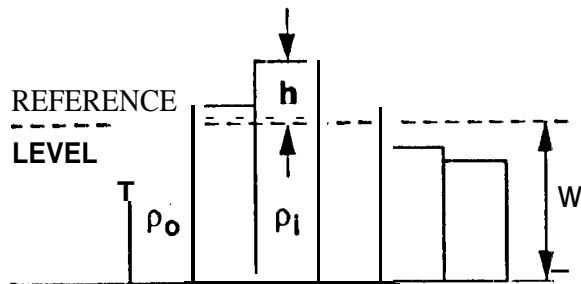


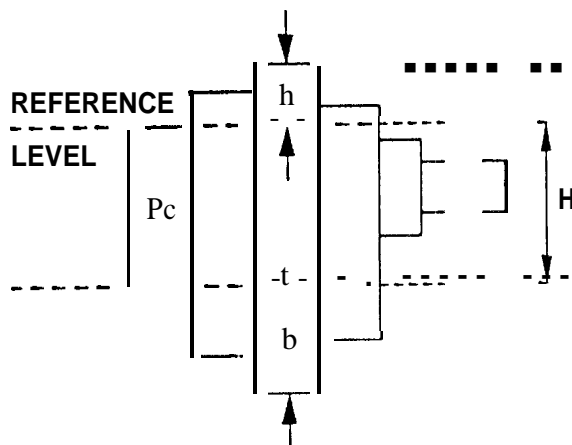
Fig. 4



a) PRATT-HAYFORD ISOSTATIC MODEL:



b) AIRY - HEISKANEN MODEL:



c) THERMAL ISOSTASY WITH LITHOSPHERIC THINNING

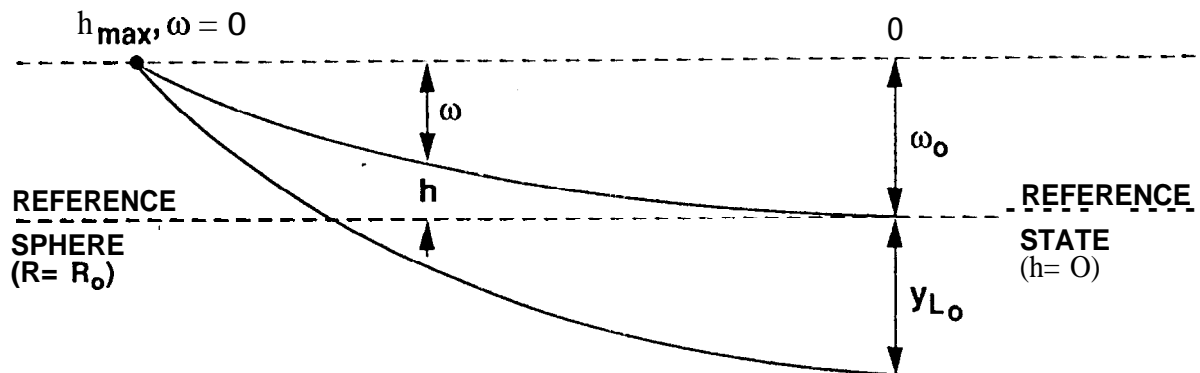


Fig. 6

REGIONAL COMPENSATION

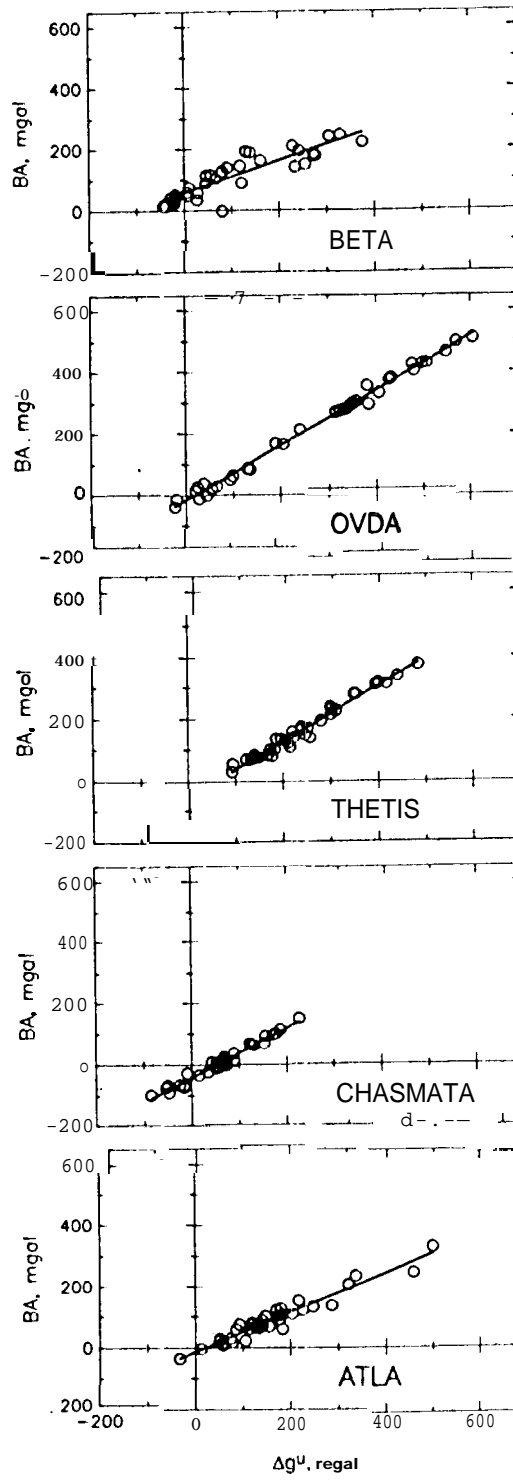
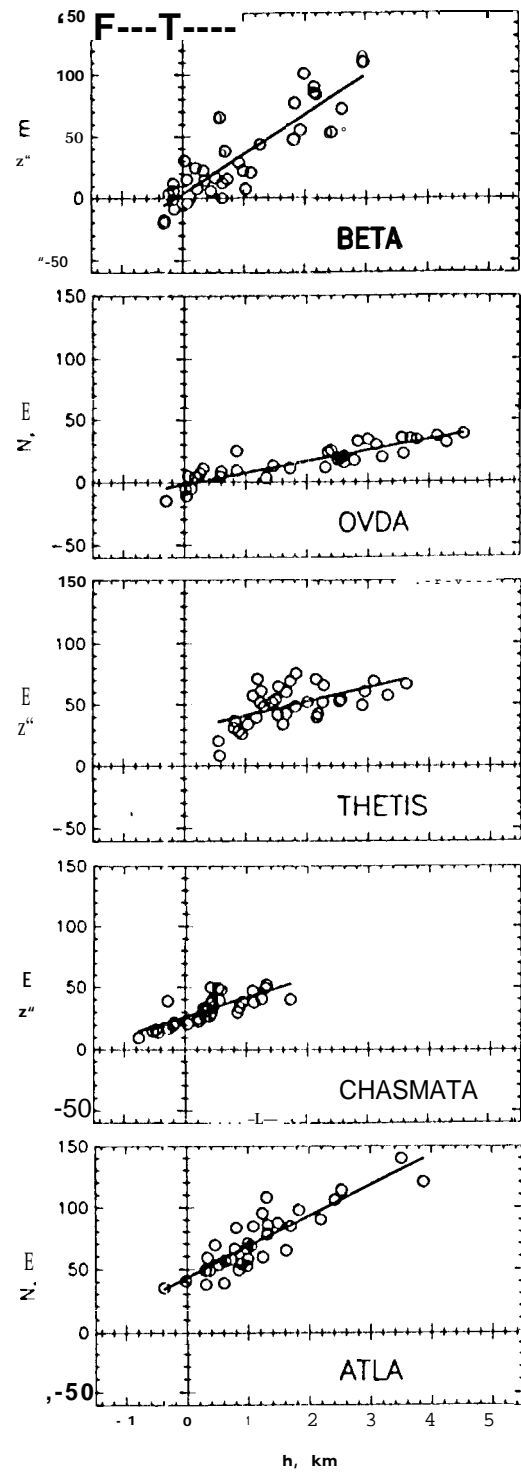


Fig. 7

a) PRATT



Fig, 8a

b) AIRY

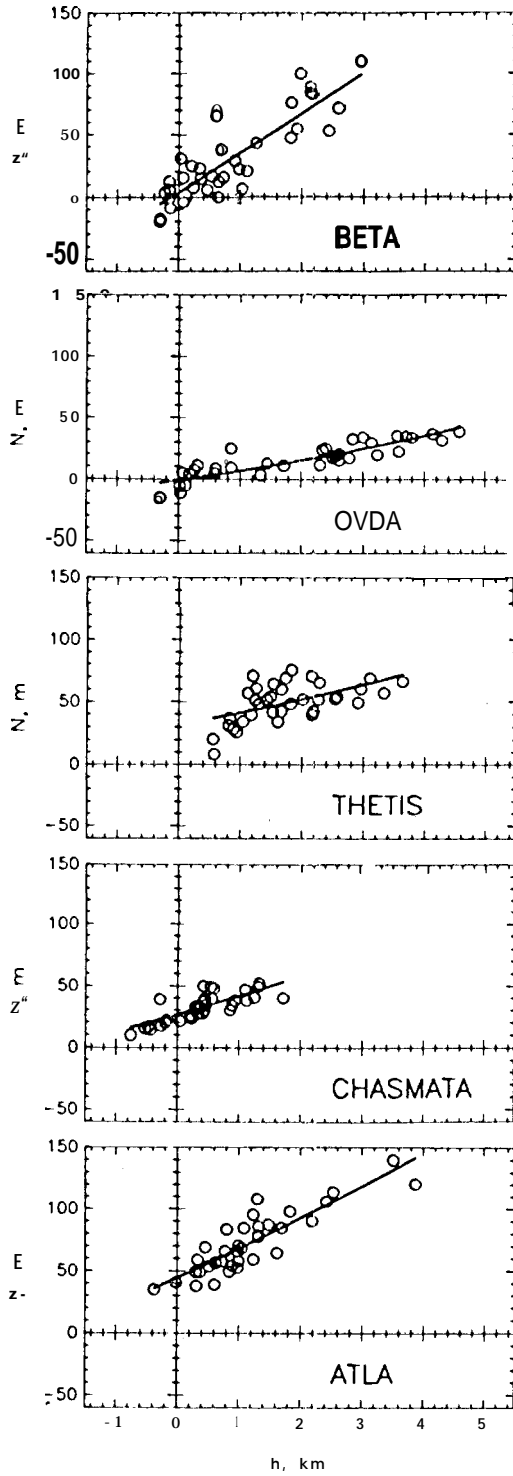


Fig. 8b

c) THERMAL

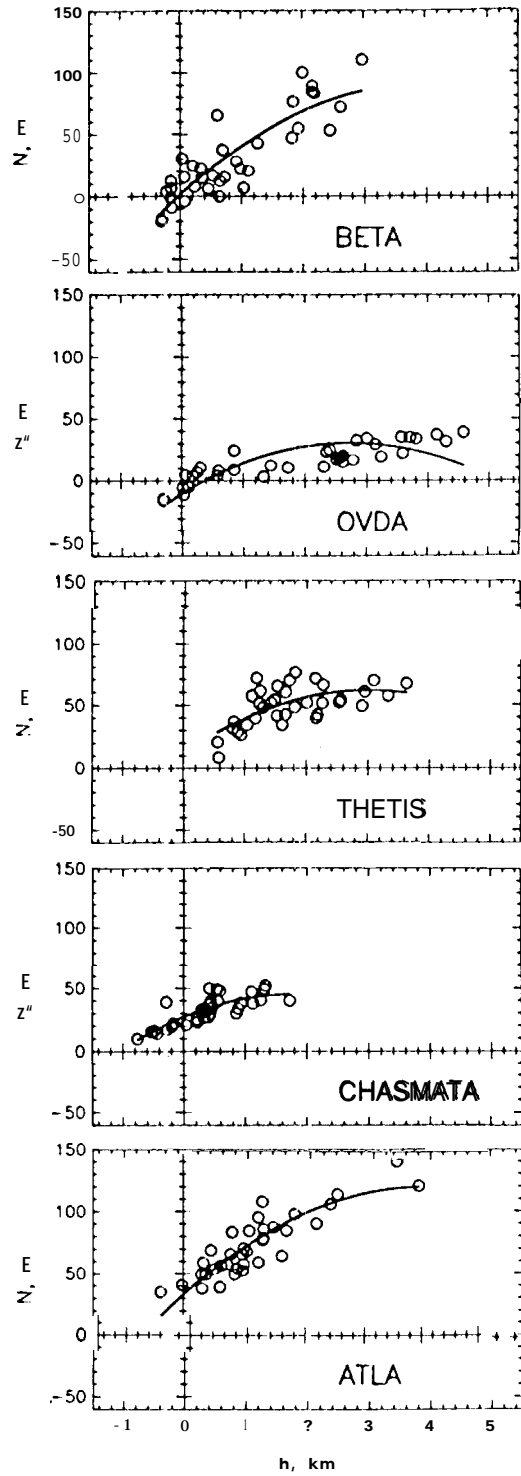


Fig. 8c